REPORT 1296

A THEORETICAL STUDY OF THE AERODYNAMICS OF SLENDER CRUCIFORM-WING ARRANGEMENTS AND THEIR WAKES [1]

By JOHN R. SPREITER and ALVIN H. SACKS

SUMMARY

A theoretical study is made of some cruciform-wing arrangements and their wakes by means of slender-body theory. The basic ideas of this theory are reviewed and equations are developed for the pressures, loadings, and forces on slender cruciform wings and wing-body combinations. The rolling-up of the vortex sheet behind a slender cruciform wing is considered at length and a numerical analysis is carried out using 40 vortices to calculate the wake shape at various distances behind an equal-span cruciform wing at 45° bank. Analytical expressions are developed for the corresponding positions of the rolled-up vortex sheets using a 4-vortex approximation to the wake, and these positions are compared with the positions of the centroids of vorticity resulting from the numerical analysis. The agreement is found to be remarkably good at all distances behind the wing.

Photographs of the wake as observed in a water tank are presented for various distances behind a cruciform wing at 0° and 45° bank. For 45° bank, the distance behind the wing at which the upper two vortices pass between the lower two is measured experimentally and is found to agree well with the 4-vortex analysis.

The calculation of loads on cruciform tails is considered in some detail by the method of reverse flow, and equations are developed for the tail loads in terms of the vortex positions calculated in the earlier analyses.

INTRODUCTION

The importance of the rolling-up of the vortex sheet in determining the downwash behind slender wings is now generally recognized and has been discussed at some length in reference 1. The current use of cruciform wings has caused the missile designer further concern regarding the downwash field in the vicinity of the tail. Such calculations are generally considerably more complicated than those for planar wings. However, since the wings on missiles of this type are generally of low aspect ratio and the tail lengths are long, it is often assumed that the vortex sheet shed from each panel of a cruciform wing is completely rolled up into a single vortex line at the tail position. One of the purposes of this paper is to investigate the usefulness of such an approximation at various distances behind the wing. This will be accomplished by comparing the results of an analytic study of the behavior of a 4-vortex model with the results of a numerical computation for a corresponding 40-vortex system and with observations of experiments conducted in a water tank.

The calculation of the pressures, loadings, and forces on cruciform wing-body combinations without regard to the wake will be treated early in the analysis, and a later section will be devoted to the calculation of the loads on a cruciform tail in the presence of the vortex wake.

PRINCIPAL SYMBOLS

A	aspect ratio
a	body radius
b	span of equal-span cruciform, $2s_o$
C_L	$\frac{L}{qS_H}$
$C_{L'}$	$\frac{L'}{qS_H}$
C_p	pressure coefficient, $\frac{p-p_\infty}{q}$
C_Y	$\frac{Y}{qS_V}$
$C_{Y'}$	$\frac{Y'}{qS_V}$
c	wing chord
d	distance behind wing trailing edge
d_L	distance behind trailing edge of cruciform wing ($\phi=45°$) at which upper two vortices pass between lower two
d_R	distance behind trailing edge at which vortices are essentially rolled up
E	elliptic integral of the second kind
F	incomplete elliptic integral of the first kind
f	lateral distance between centroids of vorticity of the two halves of the vortex wake for $\phi=45°$ ($f=y_1'+y_2'$)
$g(x)$	difference between φ and φ_2
K	complete elliptic integral of the first kind
L	force component in the z direction

[1] Supersedes NACA TN 3528 by John R. Spreiter and Alvin H. Sacks, 1956.

L'	force component in the z' direction
l	length of the airplane
M_∞	free-stream Mach number
n	outward normal from surface of airplane or wake
p	static pressure
p_∞	free-stream static pressure
q	free-stream dynamic pressure, $\frac{\rho_\infty U_\infty^2}{2}$
r	$\sqrt{y^2+z^2}$
S_c	cross-sectional area
S_H	plan form area of wing H
S_V	plan form area of wing V
s	local semispan of component wing H
s_o	maximum value of s
t	local semispan of component wing V
t_o	maximum value of t
U_∞	free-stream speed
u,v,w	fluid velocity components in the x,y,z directions
x,y,z	Cartesian coordinates fixed in the body and illustrated in figure 1.
x,y',z'	Cartesian coordinates obtained by rotating the xyz system an angle ϕ about the x axis as illustrated in figure 6
y_1',z_1', y_2',z_2'	y' and z' coordinates of vortices 1 and 2 of 4-vortex analysis
Y	force component in the y direction
Y'	force component in the y' direction
y_c,z_c	y and z coordinates of centroid of vorticity
α	angle of attack in the xyz coordinate system as illustrated in figure 1
α'	angle of attack in the $xy'z'$ coordinate system as illustrated in figure 6
β	angle of sideslip in the xyz coordinate system as illustrated in figure 1
Γ_o	maximum circulation round a wing panel
θ	angle from the positive y axis to a point on the airplane surface, positive counterclockwise, as illustrated in figure 3
λ	curve describing the cross section of the vortex wake in planes x=const.
ρ_∞	fluid mass density
σ	curve bounding the cross section of the airplane or wake in planes x=const. as illustrated in figure 2
Φ	total velocity potential
ϕ	angle of bank illustrated in figure 6
φ	perturbation velocity potential satisfying Prandtl-Glauert equation
φ_2	perturbation velocity potential satisfying two-dimensional Laplace equation in planes x=const.

SUBSCRIPTS

H	component wing lying in the xy plane
TE	wing trailing edge
u,l	two sides of the wake
V	component wing lying in the xz plane

FUNDAMENTAL RELATIONS

The theory for inviscid compressible flow about slender bodies of arbitrary cross section has become well formulated in recent years and is now described in detail in many papers (see ref. 2 or 3 for a resumé). These methods can be applied to the study of flow about cruciform wings and wing-body combinations and will be used throughout the present analysis.

THE COORDINATE SYSTEM

Most of the analysis will be referred to a Cartesian coordinate system fixed in the body, as shown in figure 1. The free-stream direction may be inclined small angles α and β with the x axis, as projected onto the xz and xy planes, respectively.

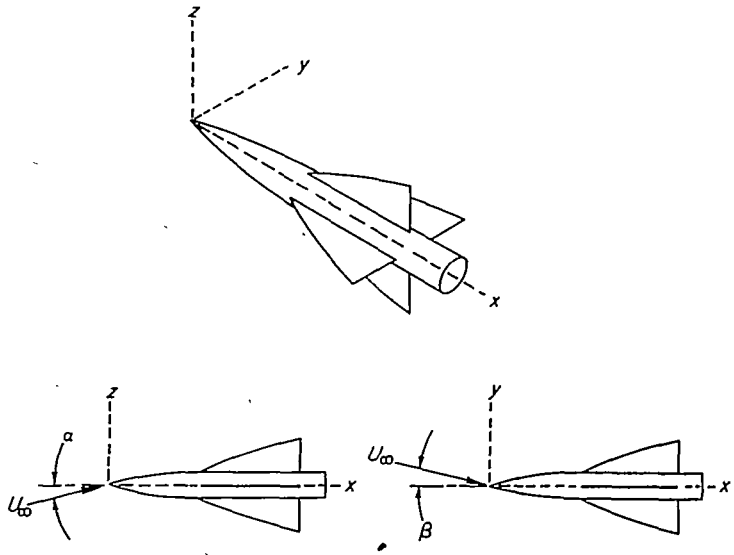

FIGURE 1.—Cruciform wing-body combination and coordinate system (xyz).

THE POTENTIAL

A perturbation velocity potential φ is introduced related to the total velocity potential Φ according to

$$\Phi=U_\infty(x-\beta y+\alpha z)+\varphi \tag{1}$$

and it is assumed that the perturbation velocities are sufficiently small that the equations for compressible flow can be satisfactorily approximated by the Prandtl-Glauert equation. Thus φ is a solution of

$$(1-M_\infty^2)\varphi_{xx}+\varphi_{yy}+\varphi_{zz}=0 \tag{2}$$

If it is assumed, furthermore, that the airplane is sufficiently slender that the longitudinal perturbation velocities and their gradients are small compared with the lateral perturbation velocities and their gradients, Ward (ref. 4) has shown that the equation for the perturbation velocity potential φ in the vicinity of the airplane is

$$\varphi=\varphi_2-\frac{U_\infty}{2\pi}\frac{\partial}{\partial x}\int_0^x \frac{dS_c}{d\xi} ln\frac{2(x-\xi)}{\sqrt{M_\infty^2-1}}d\xi \tag{3}$$

for supersonic flow ($M_\infty>1$); and Heaslet and Lomax (ref. 5) have shown that

$$\varphi=\varphi_2-\frac{U_\infty}{4\pi}\frac{\partial}{\partial x}\int_0^l \frac{dS_c}{d\xi}\frac{x-\xi}{|x-\xi|} ln\frac{2|x-\xi|}{\sqrt{1-M_\infty^2}}d\xi \tag{4}$$

for subsonic flow ($M_\infty<1$). In these equations, l represents the length of the airplane and $S_c=S_c(x)$ represents cross-sectional area in planes normal to the x axis. The symbol φ_2 in these equations represents the solution of the two-dimensional Laplace equation

$$\varphi_{yy}+\varphi_{zz}=0 \tag{5}$$

for the specified boundary conditions, and can be written explicitly as

$$\varphi_2=\frac{1}{2\pi}\int_\sigma\left(\frac{\partial\varphi}{\partial n}-\varphi\frac{\partial}{\partial n}\right)\ln r\,d\sigma \tag{6}$$

where σ is the line bounding the cross-sectional area of the airplane and its wake in the yz plane, and n is the surface normal in the yz plane, as indicated in figure 2. Thus, the three-dimensional velocity field induced by slender airplanes

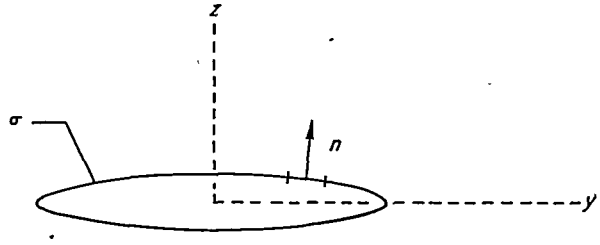

FIGURE 2.—Cross section of airplane or wake showing σ and n.

flying at either subsonic or supersonic speeds is approximated in the vicinity of the airplane and the wake by a velocity field that satisfies the two-dimensional Laplace equation and the boundary conditions in transverse planes plus a longitudinal velocity field that depends on the longitudinal rate of change of cross-sectional area and is independent of y and z. Consequently, equations (3) and (4) are often written in the following more abbreviated form

$$\varphi=\varphi_2+g(x) \tag{7}$$

which is a general solution of equation (5), but where knowledge of equation (2) must be introduced to permit the determination of $g(x)$. As is apparent from comparison of equation (7) and equations (3) and (4), the function $g(x)$ contains all of the dependence on Mach number, but the only feature of the airplane geometry which enters is the cross-sectional area. Thus, as shown by Keune (ref. 6) and Heaslet and Lomax (ref. 7), $g(x)$ for any slender airplane can be thought of as the limit for small $r=\sqrt{y^2+z^2}$ of the difference between φ and φ_2 for a body of revolution having the same $S_c(x)$ as the airplane, that is,

$$g(x)=\lim_{r\to 0}\left[-\frac{U_\infty}{4\pi}\int_0^l\frac{dS_c}{d\xi}\frac{d\xi}{\sqrt{(x-\xi)^2+(1-M_\infty^2)r^2}}-\frac{U_\infty}{2\pi}\frac{dS_c}{dx}\ln r\right] \tag{8}$$

for $M_\infty<1$ and

$$g(x)=\lim_{r\to 0}\left[-\frac{U_\infty}{2\pi}\int_0^{x-\sqrt{M_\infty^2-1}r}\frac{dS_c}{d\xi}\frac{d\xi}{\sqrt{(x-\xi)^2-(M_\infty^2-1)r^2}}-\frac{U_\infty}{2\pi}\frac{dSc}{dx}\ln r\right] \tag{9}$$

for $M_\infty>1$. It is indicated in references 8 and 9 that a corresponding relationship occurs for $M_\infty=1$ in transonic theory, although there is at present no explicit formula for computing φ for a body of revolution in transonic flow.

Once φ is determined, the pressure can be calculated directly using the relationship

$$Cp=-\frac{2}{U_\infty}(\varphi_x+\alpha\varphi_z-\beta\varphi_y)-\frac{1}{U_\infty^2}(\varphi_y^2+\varphi_z^2) \tag{10}$$

THE BOUNDARY CONDITIONS

The boundary conditions require that the gradient of the total velocity potential Φ is consistent with the free-stream conditions at infinity, and is zero when evaluated normal to and on the surface of the airplane. Consequently, φ is a constant, say zero, infinitely far ahead of and to the side of the airplane and

$$\frac{\partial\Phi}{\partial n'}=U_\infty(n_1-\beta n_2+\alpha n_3)+n_1\varphi_x+n_2\varphi_y+n_3\varphi_z=0 \tag{11}$$

on the surface of the airplane. In equation (11), n′ represents the normal to the surface, and n_1, n_2, and n_3 represent the direction cosines of n' with respect to the x, y, and z axes, respectively. By the assumptions basic to slender-airplane theory, this equation reduces to

$$U_\infty(n_1-\beta n_2+\alpha n_3)+\frac{\partial\varphi_2}{\partial n}=0 \tag{12}$$

where $\partial/\partial n=n_2(\partial/\partial y)+n_3(\partial/\partial z)$ and is the surface normal in a yz plane. Having equation (12) expressing the boundary conditions at the surface of an arbitrary slender airplane, one can easily write the corresponding relations for specific shapes. For example, the boundary condition for a body of revolution is

$$\left(\frac{\partial\varphi_2}{\partial r}\right)_{r=a}=U_\infty\left(\frac{da}{dx}-\alpha\sin\theta+\beta\cos\theta\right) \tag{13}$$

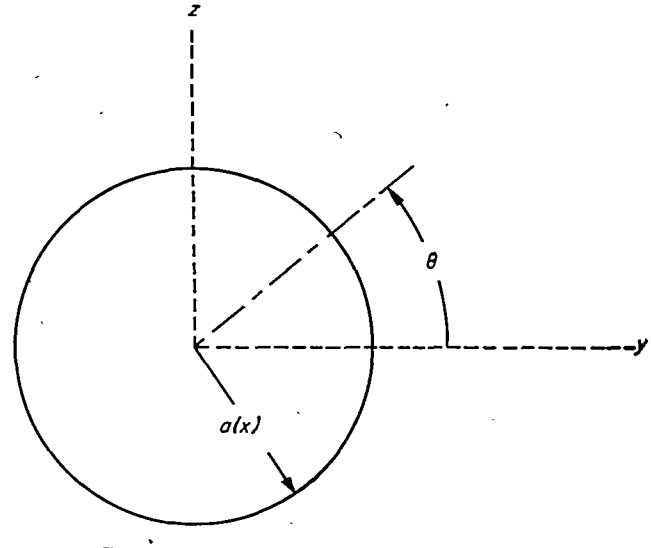

FIGURE 3.—Cross section of body of revolution showing θ and $a(x)$.

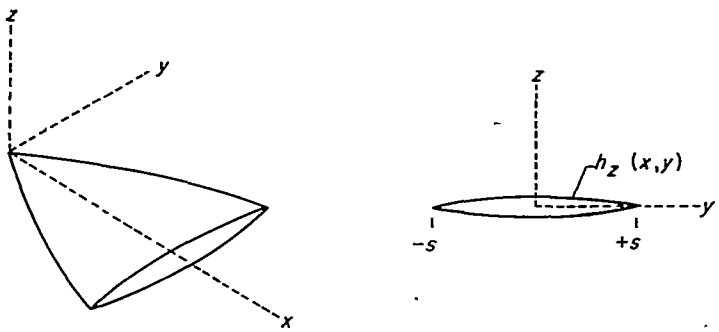

FIGURE 4.—Views of wing showing $h_z(x,y)$

where $r=a(x)$ is the body radius and θ is measured in the counterclockwise direction from the positive y axis, as shown in figure 3.

The boundary condition for a thin wing situated near the xy plane as shown in figure 4, is

$$\left(\frac{\partial\varphi_2}{\partial z}\right)_{z=0}=-U_\infty\alpha+U_\infty\frac{\partial h_z}{\partial x} \tag{14}$$

where $h_z=h_z(x,y)$ is the z ordinate of the wing surface. If the wing is situated near the xz plane, as shown in figure 5, the boundary condition is,

$$\left(\frac{\partial\varphi_2}{\partial y}\right)_{y=0}=+U_\infty\beta+U_\infty\frac{\partial h_y}{\partial x} \tag{15}$$

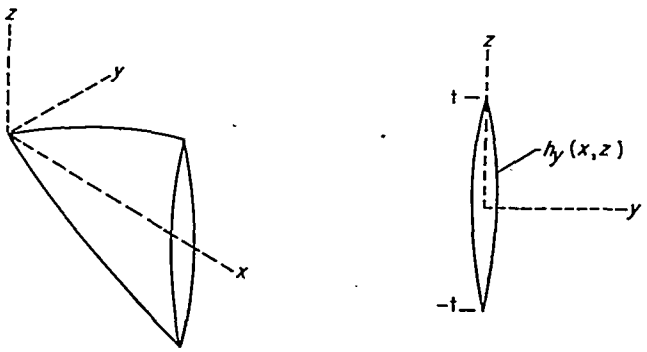

FIGURE 5.—Views of wing showing $h_y(x,z)$

where $h_y=h_y(x,z)$ now represents the y ordinate of the wing surface.

The above statements (and similar ones for other configurations) permit the determination of φ for all points in the vicinity of slender nonlifting airplanes, but only for points forward of all trailing edges for lifting airplanes. The insufficiency in the latter instance stems from the fact that the line integral in the definition of φ_2 must be carried around the trailing vortex wake and that additional relations are necessary to determine the location of the wake and the conditions existing thereon.

The vortex wake is idealized in wing theory to an infinitely thin vortex sheet extending downstream from the trailing edge of the wing. The vortex sheet can be thought of as being composed of vortex lines having constant circulation Γ, or strength, along their length. The fundamental properties are that the velocity must be purely tangential on either side of the wake, and that the pressures are equal on opposite sides of the wake. The first of these properties corresponds to the statement that $\partial\Phi/\partial n'$ is zero on both sides of the wake, and leads, in the present approximation, to equation (12). Since the direction cosines n_1,n_2, and n_3 of the normal to the wake are equal and opposite on the two sides of the wake, one concludes that $\partial\varphi_2/\partial n$ is equal and opposite on the two sides of the wake. These two properties, when combined with the pressure-velocity relation of equation (10), lead to the conclusion that the vortex lines are parallel to the average of the velocity vectors on opposite sides of the wake, again evaluated to an order consistent with the remainder of the analysis. In other words, Γ or $\Delta\varphi$ is constant along lines extending downstream from the trailing edge according to the relation

$$\frac{dy}{-U_\infty\beta+\frac{\varphi_{y_u}+\varphi_{y_l}}{2}}=\frac{dz}{U_\infty\alpha+\frac{\varphi_{z_u}+\varphi_{z_l}}{2}}=\frac{dx}{U_\infty} \tag{16}$$

where the subscripts u and l refer to the values on opposite sides of the wake. It is interesting to note in closing this discussion that the inclusion of nonlinear terms in the pressure-velocity relation of slender-wing theory requires consideration of the deformation and rolling-up of the vortex wake, and that the flat wake commonly assumed in linear theory is inconsistent with the use of equation (10) for the pressure. Additional discussion of these points can be found in reference 3.

A SECOND COORDINATE SYSTEM

In order to take advantage of certain symmetry properties, part of the results will be given in terms of a second coordinate system $xy'z'$. This coordinate system is related to the xyz system by such a rotation about the x axis that the xz' plane contains both the x axis and the free-stream direction. With this system, the airplane is banked an angle ϕ with respect to the y' axis, and the free-stream direction makes an angle α' with the x axis as shown in figure 6. Since α and β are small angles, we have the following relations:

$$\phi=\tan^{-1}\frac{\beta}{\alpha},\qquad \alpha'=\sqrt{\alpha^2+\beta^2} \tag{17}$$

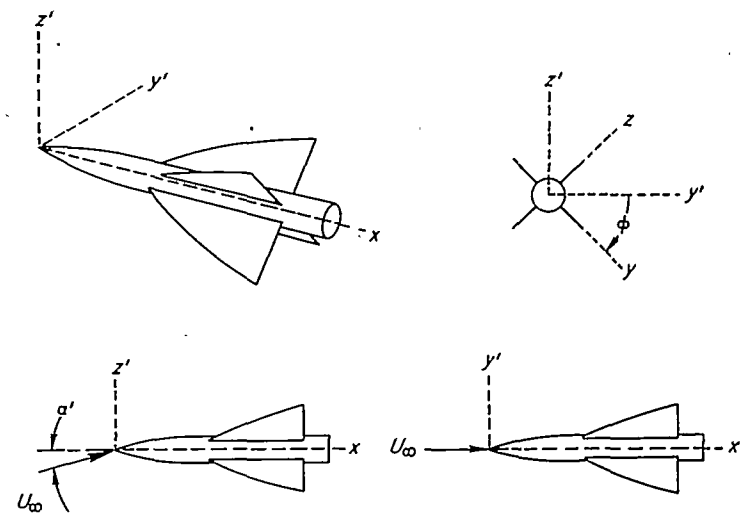

FIGURE 6.—Cruciform wing-body combination and rotated coordinate system ($xy'z'$).

This coordinate system will be used from time to time during the discussion and for the presentation of the specific results for $\phi=45°$.

FORCES ON SLENDER CRUCIFORM WINGS

The relationships outlined in the preceding section apply to slender bodies of arbitrary cross section. Inasmuch as the vortex calculations, which are the principal subject of this study, are confined to cases involving either plane or cruciform arrangements of thin wings, attention will be devoted in this section to the determination of the aerodynamic forces on flat-plate wings of zero thickness. (The corresponding results for slender wing-body combinations are included in the appendix.) These results supersede those of reference 10 in which proper account is not taken of the nonlinear terms in the pressure coefficient. Thus, consider the cruciform wing illustrated in figure 7 and designate the

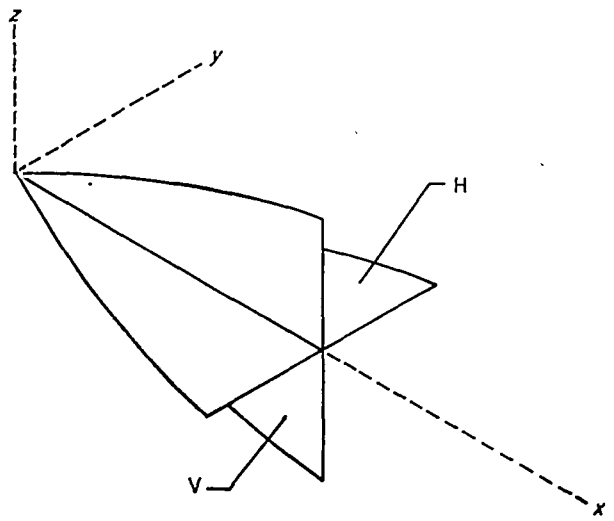

FIGURE 7.—Designation of cruciform surfaces.

component wing which extends along the y axis as H and that which extends along the z axis as V. Both components are symmetrical about the x axis, the plan form of wing H being given by $y=\pm s(x)$ and that of wing V by $z=\pm t(x)$. Since the wings have no thickness, $g(x)=0$, the flow is unaffected by Mach number, and $\varphi=\varphi_2$. The solution for this case can be considered to be the sum of the solutions for the flows about each component alone as shown in figure 8,

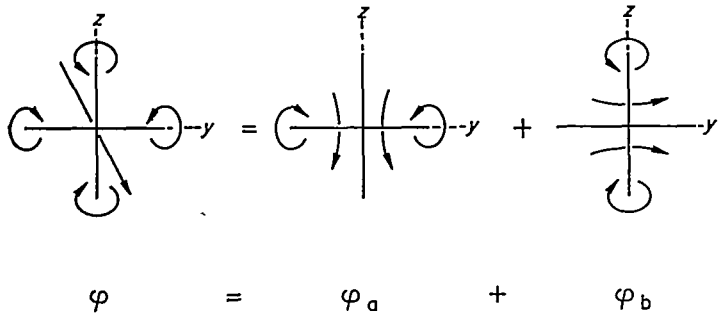

FIGURE 8.—Addition of potentials for cruciform wing.

since wing H lies in a plane of symmetry of the perturbation flow φ_b about wing V, and wing V lies in a plane of symmetry of the perturbation flow φ_a about wing H. The expression for φ_a can be found in many sources (e. g., ref. 11) and is

$$\varphi_a=\pm\frac{U_\infty\alpha}{\sqrt{2}}\sqrt{s^2-y^2+z^2+\sqrt{(s^2-y^2+z^2)^2+4y^2z^2}}-U_\infty\alpha z \quad (18)$$

where the sign is positive in the upper half-plane and negative in the lower half-plane. The expression for φ_b is

$$\varphi_b=\pm\frac{U_\infty\beta}{\sqrt{2}}\sqrt{t^2+y^2-z^2+\sqrt{(t^2+y^2-z^2)^2+4y^2z^2}}+U_\infty\beta y \quad (19)$$

where the sign is positive in the left half-plane and negative in the right half-plane. The perturbation velocity potential for the flow about the cruciform wing is thus

$$\varphi=\varphi_a+\varphi_b \quad (20)$$

Through application of equations (10) and (18) through (20), expressions for the differential pressures or loadings on the two component wings are found to be

$$\left.\begin{aligned}\left(\frac{\Delta p_L}{q}\right)_H&=\frac{4\alpha ds/dx}{\sqrt{1-y^2/s^2}}+\frac{4\alpha\beta y/s}{\sqrt{1-y^2/s^2}}\frac{1}{\sqrt{1+t^2/y^2}}\\ \left(\frac{\Delta p_Y}{q}\right)_V&=-\frac{4\beta dt/dx}{\sqrt{1-z^2/t^2}}+\frac{4\alpha\beta z/t}{\sqrt{1-z^2/t^2}}\frac{1}{\sqrt{1+s^2/z^2}}\end{aligned}\right\} \quad (21)$$

The sign convention is such that the loadings are positive when they are associated with forces in the direction of the positive y and z axes, and hence with positive lift and side force as indicated by the subscripts on the symbol Δp.

Of the two terms in the loading expressions, the symmetric first terms contribute to lift and side force and the antisymmetric second terms contribute to rolling moment. To illustrate this point further, figure 9 shows the load distribution on a cruciform wing having triangular components. The loading on the vertical component is shown by the two

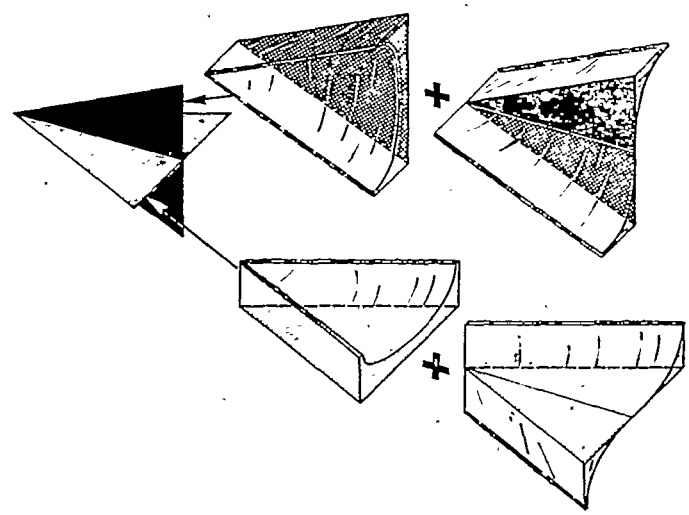

FIGURE 9.—Load distributions on triangular cruciform wing components.

top sketches, and that on the horizontal component is shown by the lower sketches. The sketches on the left represent the contribution of the symmetric first terms of equation (21); those on the right, the contribution of the antisym-

metric second terms. As has been pointed out in many discussions of slender-wing theory, equation (21) for the loading applies only to those portions of wings for which ds/dx and dt/dx are positive. Consequently, the present analysis will be confined to wings having their maximum span at the trailing edge. The permissible ranges for α and β are also restricted inasmuch as equation (21) becomes invalid when either the angle of pitch or yaw becomes so large that the leading edge rotates beyond the free-stream direction and becomes, effectively, a trailing edge. Mathematically, this limit occurs when $|\beta|=ds/dx$ and when $|\alpha|=dt/dx$. If it is desired to investigate wings inclined at large angles, consideration must be given to the influence of the trailing vortices lying outboard of the sides of the wing.

The total forces on the cruciform wing can be determined by integrating the loading over the entire surface area. Thus, the lift (i. e., the total force in the direction of the positive z axis) is given by

$$L=\iint_H \Delta p_L\,dx\,dy+2\pi q\alpha s_o^2 \tag{22}$$

where s_o is the maximum semispan of wing H. Likewise, the total side force in the direction of the positive y axis is

$$Y=\iint_V \Delta p_Y\,dx\,dz=-2\pi q\beta t_o^2 \tag{23}$$

where t_o is the maximum semispan of wing V. The same results, expressed in coefficient form, are

$$C_L=\frac{L}{qS_H}=\frac{\pi}{2}A_H\alpha \tag{24}$$

$$C_Y=\frac{Y}{qS_V}=-\frac{\pi}{2}A_V\beta \tag{25}$$

It may be noted that these latter integrated results can be obtained more easily by momentum methods (e. g., refs. 2 and 3) if details of the loadings are not required. For example, the lift of any plane or cruciform wing is given simply by

$$L=\rho_\infty U_\infty\int_{-s_o}^{+s_o}\Delta\varphi_{TE}\,dy \tag{26}$$

where $\Delta\varphi_{TE}$ refers to the difference in the values of the perturbation potential φ on the two sides of the wing, evaluated at the trailing edge.

WAKE AND DOWNWASH

The determination of the shape of the trailing vortex sheet and the associated velocity field behind a wing customarily involves considerations of classical vortex laws together with the known vorticity distribution at the trailing edge. For slender wings, these relations are all imbedded in the equations given in the first section of the present analysis. Thus, since $S_c=0$ behind the wing and $\partial\varphi/\partial n$ is equal and opposite on the two sides of the vortex wake, it follows from equations (3), (4), and (6) that the perturbation potential for the flow in any lateral plane behind the wing is given by

$$\varphi=\varphi_2=-\frac{1}{2\pi}\int_\sigma\varphi\frac{\partial}{\partial n}\ln r\,d\sigma \tag{27}$$

A direct consequence of the zero thickness of the vortex wake is that the normal derivative in equation (27) is equal and opposite on the two sides of the wake. This means that the contour integral around the wake indicated by σ in equation (27) can be replaced with a line integral along only one side λ of the vortex sheet. The integrand then involves not φ, but the difference in potential $\Delta\varphi$ on the two sides of the wake. Since, furthermore

$$\Delta\varphi=\Gamma \tag{28}$$

and

$$\frac{\partial}{\partial n}\ln r=-\frac{\partial}{\partial\lambda}\tan^{-1}\frac{z-z_1}{y-y_1} \tag{29}$$

equation (27) becomes, on performing an integration by parts

$$\varphi=\frac{1}{2\pi}\int_\lambda\Gamma\frac{\partial}{\partial\lambda}\tan^{-1}\frac{z-z_1}{y-y_1}\,d\lambda=-\frac{1}{2\pi}\int_\lambda\frac{\partial\Gamma}{\partial\lambda}\tan^{-1}\frac{z-z_1}{y-y_1}\,d\lambda \tag{30}$$

since Γ is zero at the lateral extremities of the vortex sheet. The corresponding relations for the velocity components v and w in the direction of the positive y and z axes can be found by using equation (30) in conjunction with equation (1), thus

$$v=\frac{\partial\Phi}{\partial y}=-U_\infty\beta+\varphi_y=-U_\infty\beta+\frac{1}{2\pi}\int_\lambda\frac{\partial\Gamma}{\partial\lambda}\frac{z-z_1}{(y-y_1)^2+(z-z_1)^2}\,d\lambda \tag{31}$$

$$w=\frac{\partial\Phi}{\partial z}=U_\infty\alpha+\varphi_z=U_\infty\alpha-\frac{1}{2\pi}\int_\lambda\frac{\partial\Gamma}{\partial\lambda}\frac{y-y_1}{(y-y_1)^2+(z-z_1)^2}\,d\lambda \tag{32}$$

The relation for the path of each vortex line given by equation (16) can be expressed in terms of v and w, thus

$$\frac{dy}{\left(\frac{v_u+v_l}{2}\right)}=\frac{dz}{\left(\frac{w_u+w_l}{2}\right)}=\frac{dx}{U_\infty} \tag{33}$$

where the subscripts u and l again refer to the values on the two sides of the vortex wake.

The principal difficulty in the calculation of v and w stems from the fact that the shape λ and the vorticity distribution $\partial\Gamma/\partial\lambda$ of the wake are not immediately known at all stations behind the wing, but only at the trailing edge. At this station, the circulation distribution can be determined directly from equations (18) through (20) by setting $z=0$ for the vortex sheet behind wing H and $y=0$ for that behind wing V and replacing s and t with s_o and t_o (the maximum values for s and t, occurring at the trailing edge). The resulting expressions

$$\Gamma_H=\Delta\varphi_H=2U_\infty\alpha\sqrt{s_o^2-y^2} \tag{34}$$

$$\Gamma_V=\Delta\varphi_V=2U_\infty\beta\sqrt{t_o^2-z^2} \tag{35}$$

indicate that the circulation distribution is elliptic immediately behind each wing. This case illustrates the fact that the circulation distribution and span loading are not always

proportional. This conclusion is immediately apparent when it is observed that the circulation distribution for the present case is symmetric about the x axis, whereas the span loading is asymmetric, as can be seen by examining figure 9. If attention is confined to stations immediately behind the trailing edge and to cases where the wing is at very low lift, so that $x-x_{TE}$ and Γ are small, it may be assumed for certain purposes that the distortion and rolling-up of the wake are so slight that they can be disregarded. With this assumption, the induced flow field behind a lifting wing can be computed directly. Thus, the perturbation potential for the flow behind the triangular cruciform wing treated in the preceding section can be obtained from equations (18) through (20) by again substituting s_o for s and t_o for t, and the associated velocity field can be found therefrom by differentiation. Although the error incurred in the induced velocities by the use of this assumption can be continually diminished as the lift and distance from the wing is reduced, the condition of zero force on the wake is always violated at the edges of the wake. The elimination of these forces demands that the vortices be free to roll up. Inasmuch as these effects become of increasing importance as the aspect ratio is decreased, attention here will be focused more on determining the behavior of the trailing vortex system than on performing calculations assuming a simplified wake form.

SIMILARITY CONSIDERATIONS

The rate at which distortion of the wake progresses with increasing distance from the wing will first be investigated by means of similarity considerations. Consider two geometrically similar cruciform wings traveling at either subsonic or supersonic speeds, but differing in span and angles of pitch and yaw. It is desired to relate the distances behind the two wings at which the wake patterns are similar. Let the symbols referring to the reference wing be denoted by asterisks and those referring to the second wing be plain. Inasmuch as a first requirement is that the vorticity distributions must be similar at the trailing edge, it is necessary that the ratio of angle of attack to angle of sideslip α/β be the same for both wings. (If the problem is stated in the alternative manner by specifying the angle of attack α' and angle of bank ϕ, this condition corresponds to requiring that both wings have the same angle of bank.) From equations (31) and (32), it is evident that the perturbation velocity components φ_y and φ_z behind the wing are directly proportional to the circulation and inversely proportional to the scale. Inasmuch as the former is measured by, say, the maximum value of the circulation Γ_o, and the latter by the semispan s_o, the ratio of the lateral induced velocities at corresponding stations behind the wings is equal to the ratio of the circulation loading of the two wings.

$$\frac{\varphi_y}{\varphi_y^*}=\frac{\varphi_z}{\varphi_z^*}=\frac{\Gamma_o/s_o}{\Gamma_o^*/s_o^*} \tag{36}$$

Since the ratio of the longitudinal distances, in terms of wing semispans, from the trailing edge to stations having similar wake patterns is inversely proportional to the ratio of the induced velocities, in terms of the free-stream velocity, we have

$$\frac{d/s_o}{d^*/s_o^*}=\frac{U_\infty/\varphi_y}{U_\infty^*/\varphi_y^*}=\frac{U_\infty s_o\Gamma_o^*}{U_\infty^* s_o^*\Gamma_o} \tag{37}$$

This relation reduces to the following when the circulation function Γ_o is replaced by the lift L through the introduction of equation (26)

$$\frac{d/s_o}{d^*/s_o^*}=\frac{\rho_\infty U_\infty^2 s_o^2 L^*}{\rho_\infty^* U_\infty^{*2} s_o^{*2} L} \tag{38}$$

or in dimensionless form

$$\frac{d/s_o}{d^*/s_o^*}=\frac{A/C_L}{A^*/C_L^*} \tag{39}$$

where A refers to the aspect ratio and C_L to the lift coefficient. In many cases, it is preferred to express the distance d in terms of the wing chord rather than the semispan, whence

$$\frac{d/c}{d^*/c^*}=\frac{A/C_L}{A^*/C_L^*}\frac{s_o/c}{s_o^*/c^*} \tag{40}$$

From this result, it can be concluded that the expression for the distance required for the trailing vortex sheets to assume any particular configuration is of the form

$$\frac{d}{c}=k\left(\frac{A}{C_L}\right)\left(\frac{2s_o}{c}\right) \tag{41}$$

where k is, as yet, an unspecified constant. This formula is directly applicable to both the rolling-up of the vortex sheets and the relative motions of the rolled-up vortices. Thus, for instance, one set of values for k will give the distance required for the vortex sheets to become rolled up to any given degree as a function of the angle of bank ϕ; whereas another set of values will give the distance for the rolled-up vortices to assume some particular orientation with respect to one another.

The foregoing analysis gives no information regarding the relative rates of rolling-up of the individual vortex sheets trailing from each panel of a cruciform wing. If the angle of sideslip β is zero and the angle of attack is different from zero (or the angle of bank ϕ is zero), a vortex sheet exists at the trailing edge of only the horizontal wing and it rolls up in exactly the same manner as it does behind a single plane wing. If, on the other hand, the angles of attack and sideslip are equal (or the angle of bank is 45°) and the cruciform wing is composed of four identical panels, the vorticity distribution at the trailing edge of each panel is the same and the wake rolls up into four equal vortices at nearly equal rates. Other cases are more complicated.

Attention has been called in reference 1 and elsewhere to the value of $k=0.28$ given by Kaden in reference 12 for the constant in equation (41) for the distance required for the vortex sheet trailing from a plane wing having elliptic circulation distribution to become "essentially rolled up." Although the accuracy, as well as the precise meaning of Kaden's result is impaired by the numerous and somewhat arbitrary assumptions introduced in the course of the analysis, the result is useful for predicting the order of magnitude of the distance involved. The problem actually attacked by Kaden is that of the rolling up of a vortex sheet of semi-infinite width, having parabolic circulation distri-

bution. The result is applied to the case of a vortex sheet of finite width having elliptic circulation distribution by selecting the strength of the parabolic distribution to match the known elliptic distribution at the wing tip, and assuming that the rolling up of the finite vortex sheet and the semi-infinite sheet proceed identically.

If the same ideas together with Kaden's result for the plane wing are applied to the cruciform wing, the distance from the trailing edge to the station where the vortices are essentially rolled up is

$$\left(\frac{d_R}{c}\right)_H = 0.28 \frac{A}{C_L} \frac{2s_o}{c} \tag{42}$$

for the horizontal wing and

$$\left(\frac{d_R}{c}\right)_V = 0.28 \frac{A}{C_Y} \frac{2t_o}{c} \tag{43}$$

for the vertical wing.

NUMERICAL RESULTS (20 AND 40 VORTICES)

A detailed analysis of the form of the vortex system behind lifting wings can be made on the basis of equations (31) through (33) by replacing the continuous sheet of vortices with a finite number of discrete vortices and determining their positions at each longitudinal station by a step-by-step calculation procedure. Such a calculation was carried out long ago by Westwater (ref. 13) for the plane wing with elliptic circulation distribution. In this particular treatment, the vortex sheet was replaced by 20 vortices of equal strength and the results were presented by giving, both numerically and graphically, the positions of each of the vortices at several different distances behind the wing. These results, which of course apply equally to cruciform wings at zero sideslip, are summarized in graphical form in figure 10. Although these results are presented here in terms of body axes, rather than wind axes as previously given in reference 1, additional reference lines are included which extend downstream from the trailing edge in the free-stream direction. This sketch clearly illustrates how the center of the vortex sheet behind low-aspect-ratio wings extends downstream in nearly the direction of the extended chord plane, while the vortex cores extend downstream in nearly the direction of the free stream. Similar calculations have been made recently for wing-body combinations and are reported in reference 14 by Rogers.

A numerical calculation [2] has been carried out for the case of a cruciform wing having four identical panels at equal angles of attack and sideslip ($\phi=45°$). In this calculation, the vortex sheet trailing from each of the four panels is replaced by 10 discrete vortices of equal strength distributed in such a fashion that the area under each step of the approximate circulation distribution is equal to that under the corresponding portion of the elliptic curve representing the given circulation distribution. With the strengths and positions of the vortices thus determined, the velocity com-

[2] The actual computations were done under the supervision of Mr. Stewart M. Crandall of the Electronic Machine Computing Branch of the Ames Aeronautical Laboratory.

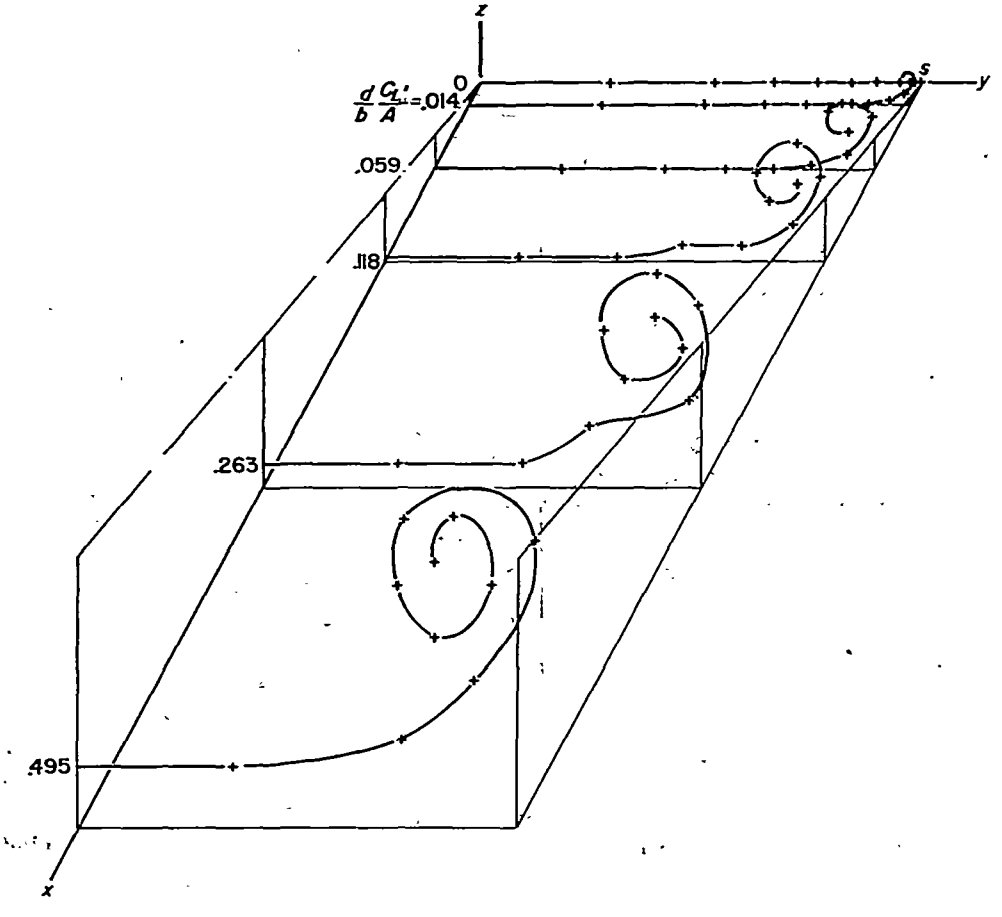

FIGURE 10.—Shape of vortex sheet for plane wing with elliptic circulation distribution.

ponents at the position of each vortex are computed using equations (31) and (32) and the change in the position of the vortices with a small increase of the distance from the wing is determined using equation (33). This process is then repeated using the new vortex positions. Since the entire trailing vortex system is symmetrical about a line inclined at 45° to the xyz coordinate system the results are expressed in terms of the $xy'z'$ coordinate system described earlier with the angle of bank ϕ set equal to 45°. With the positions of the vortices given in this system, it is necessary to specify the coordinates of only half the vortices, since the strengths and locations of the remainder are just those of mirror images about $y'=0$; that is, with the vortices numbered from 1 through 40 as indicated in figure 11, vortex $20+i$ is the image of vortex i and the following relations hold between the two vortices.

$$z'_{20+i}=z_i';\ y'_{20+i}=-y_i';\ \Gamma_{20+i}=-\Gamma_i \tag{44}$$

Since the force component in the direction of the y' axis, or the side force Y', vanishes, the force component in the direction of the z' axis, or the lift L', is equal to the resultant lateral force, thus

$$L'=\sqrt{L^2+Y^2}=\sqrt{2}L \tag{45}$$

or, in coefficient form

$$C_L'=\frac{L'}{qS_H}=\sqrt{2}C_L \tag{46}$$

Since it follows, furthermore, from equation (17) that

$$\alpha'=\sqrt{\alpha^2+\beta^2}=\sqrt{2}\alpha \tag{47}$$

we have

$$C_L'=\frac{\pi}{2}A_H\alpha'=\frac{\pi}{2}A_V\alpha';\ C_Y'=0 \tag{48}$$

for cruciform wings of equal span.

The results of the calculations are given in three forms. A highly abridged illustration of the results is given in figure 12, a more complete series of illustrations is provided in figure 13, and a complete listing of the numerical results is given in table I. In order to facilitate the fairing near the plane of symmetry of the curves representing the vortex wake, the position of the point lying in the plane of symmetry was calculated at each downstream station. In keeping with the remainder of the present analysis, the above results are given in terms of body axes. Additional reference marks are shown on the graphical presentations, however, to indicate the position of a line in the free-stream direction passing through the trailing edge of the wing root. In figure 12, this line is shown as a solid line lighter in weight than the axes. In figure 13, its position is indicated by a small circle on the z' axis. As can be seen from examination of the results, these calculations were carried forth for distances behind the wing up to approximately an $(A/C_L')(b/c)$ of unity. The rolling up of the vortex sheets is clearly evident and has progressed to a substantial extent at the most rearward station. Attention is called to the fact that this distance is much greater than that indicated by Kaden's formulas for the distance to roll up and that the rolling up of the vortex sheets proceeds at a much slower rate than indicated by these relations. The same conclusions follow from an examination of the planar case.

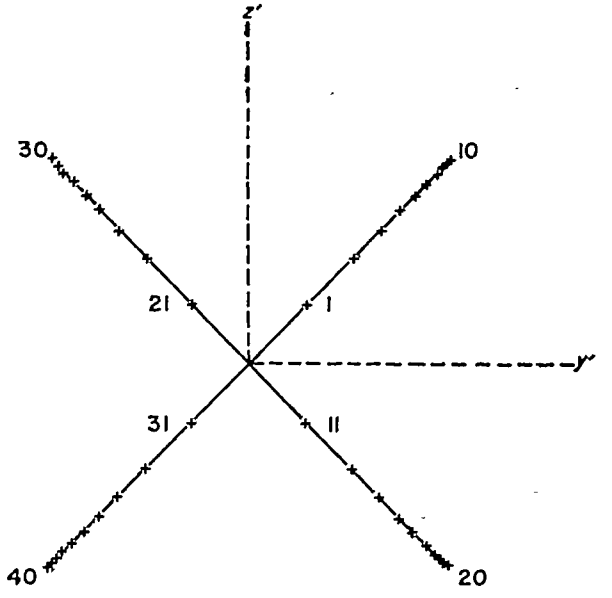

FIGURE 11.—Numbering system for 40-vortex calculations.

A second prominent feature of the vortex wake of cruciform wings at 45° bank concerns the tendency of the vortices from the upper wing panels to incline downward toward those from the lower wing panels, and eventually to pass between them. Although the present calculations were not carried on to sufficiently large distances from the wing to display this phenomenon fully, the results do confirm the conclusions of reference 15 that this "leapfrog" distance is much greater than the distance indicated by Kaden's formula for rolling up of the vortex sheets. An important consequence of the difference in these distances is that the full details of the rolling up need not be considered in the analysis of the slower leapfrog phenomenon. Thus, if the properties of a continuous vortex system are to be ascertained by considering the properties of a system comprised of a finite number of discrete vortices, a great many vortices are necessary to trace the course of the rolling up, whereas a satisfactory model for studying the leapfrog characteristics may often be had by using only one vortex per wing panel.

ANALYTICAL RESULTS (4 VORTICES)

It is apparent from the preceding discussion that a very large number of discrete vortices must be included to give an adequate representation of the vortex system near the wing. At greater distances from the wing where the vortex sheets are substantially rolled up, it appears plausible that the analysis can be simplified, while still retaining the essential features, by assuming that the vortex sheets are fully rolled up into four vortex lines (one from each wing panel). This simplification is analogous to the use of a vortex pair for calculating the induced flow field at great distances behind a lifting planar wing.

In contrast to the case of the plane wing for which the vortex sheet rolls up into two vortex lines that, at great distance behind the wing, are simply straight lines inclined at a small angle from the free-stream direction, the analogous

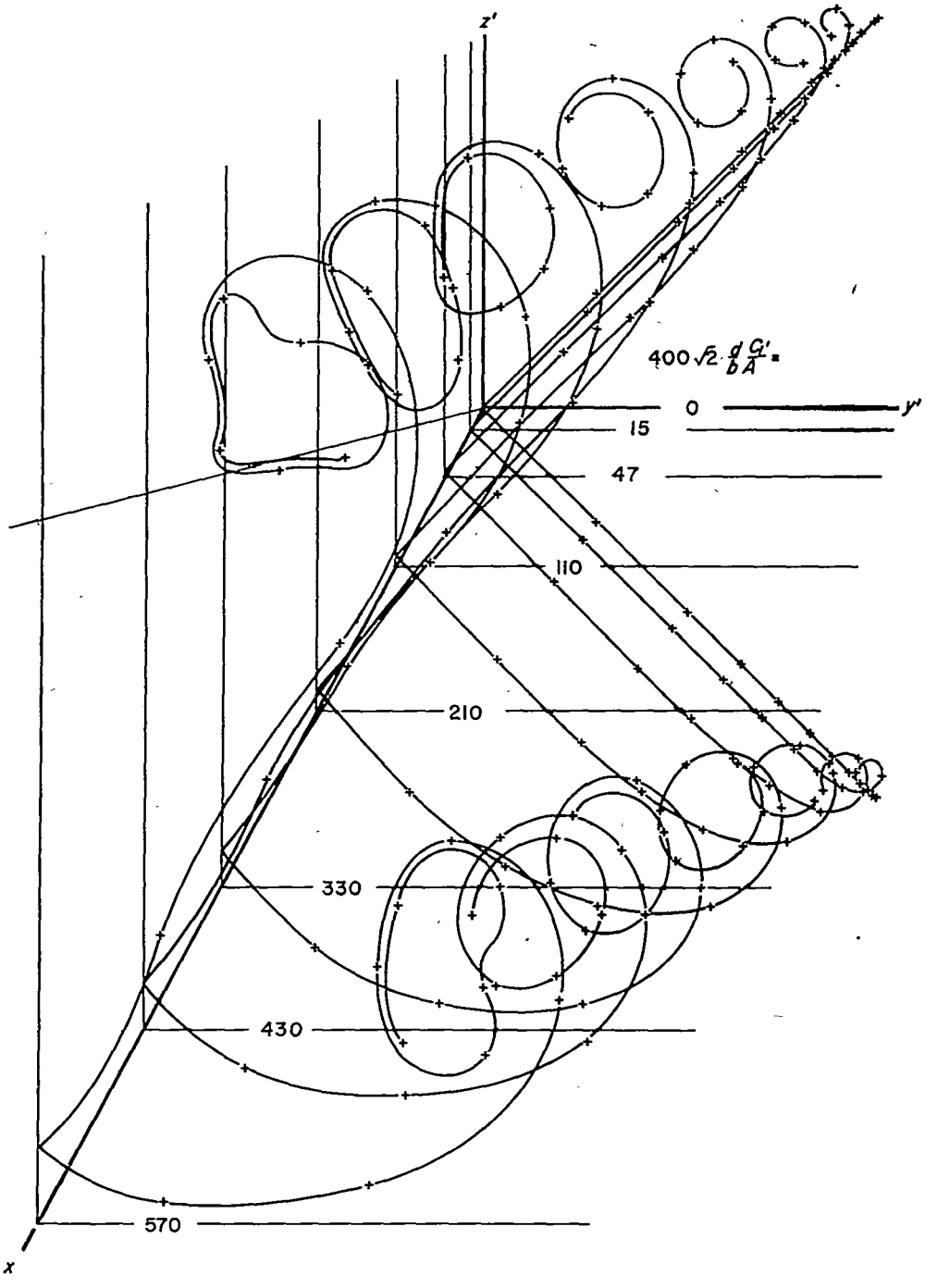

FIGURE 12.—Shape of vortex sheets for cruciform wing at 45° bank with elliptic circulation distribution.

problem for cruciform wings is necessarily more complicated. Instead of two rolled-up vortices, there are now four and their induced effects upon one another are such that the curves described by the vortex lines are quite intricate. The simplification introduced by diminishing the number of vortices from 40, say, to 4, however, is particularly important since it permits the use of analytical methods instead of the numerical procedures described in the preceding sections.

The first step in the development of this analysis is to select the strengths and locations of the four vortices used to represent the actual vortex sheet at the wing trailing edge. Since it is assumed that all of the vorticity from each wing panel rolls up into a single vortex, it appears natural to consider that each vortex is of strength equal to the circulation around the corresponding wing panel and is situated laterally, at the trailing-edge station, at the position of the centroid of vorticity of the vortex sheet it replaces. It is further assumed that the strength of each vortex is constant along its length, but that its lateral position changes with x in accordance with the velocities induced by the other three vortices. Although coincidence of the lateral position of each of the four discrete vortices of the simplified model and the centroid of vorticity of each of the actual vortex sheets is assured at only the trailing edge of the wing, it is tacitly assumed that the two sets of locations are sufficiently near to be interchangeable for most practical purposes. The accuracy of

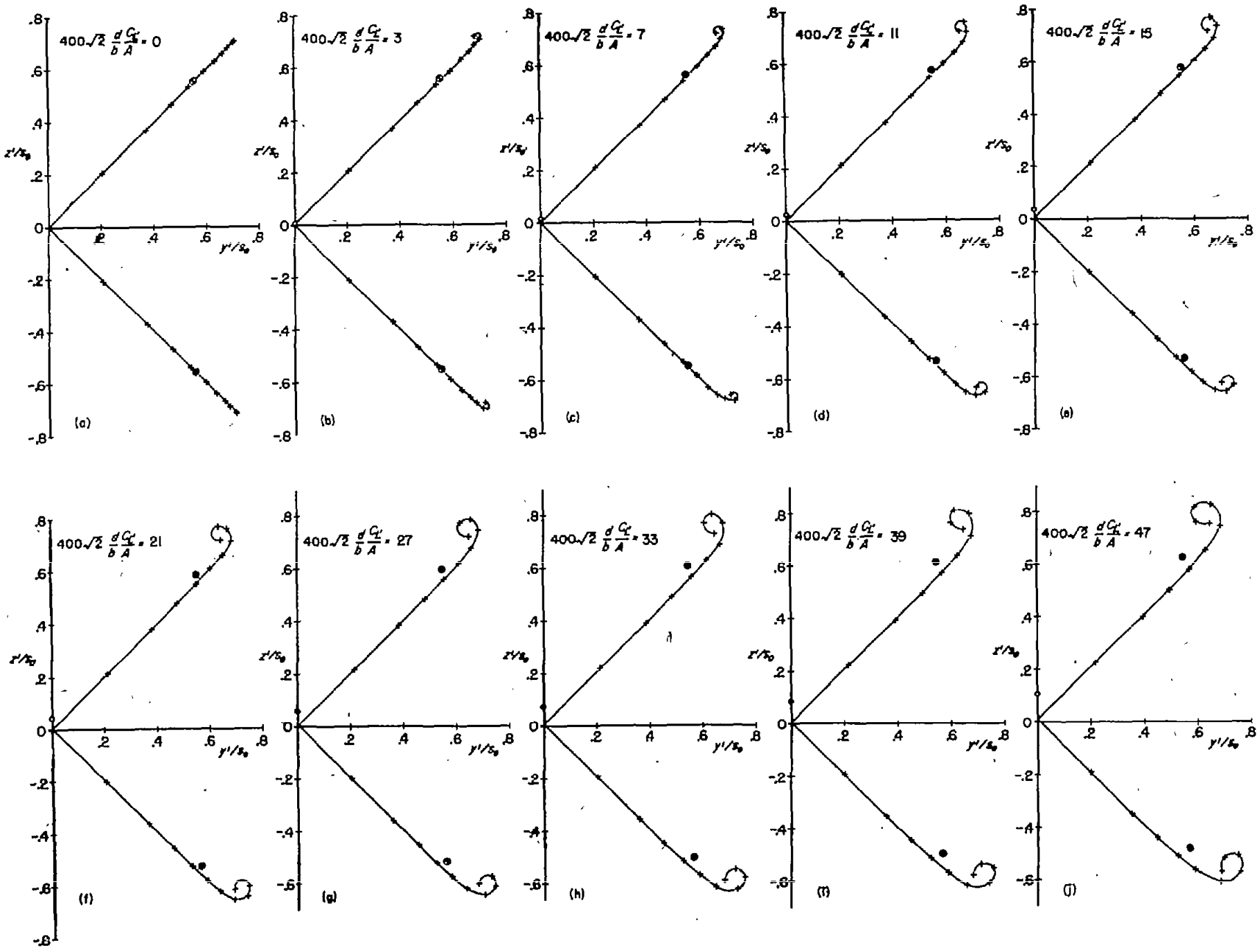

FIGURE 13.—Calculated wake shape at various distances behind an equal-span cruciform wing; $\phi = 45°$

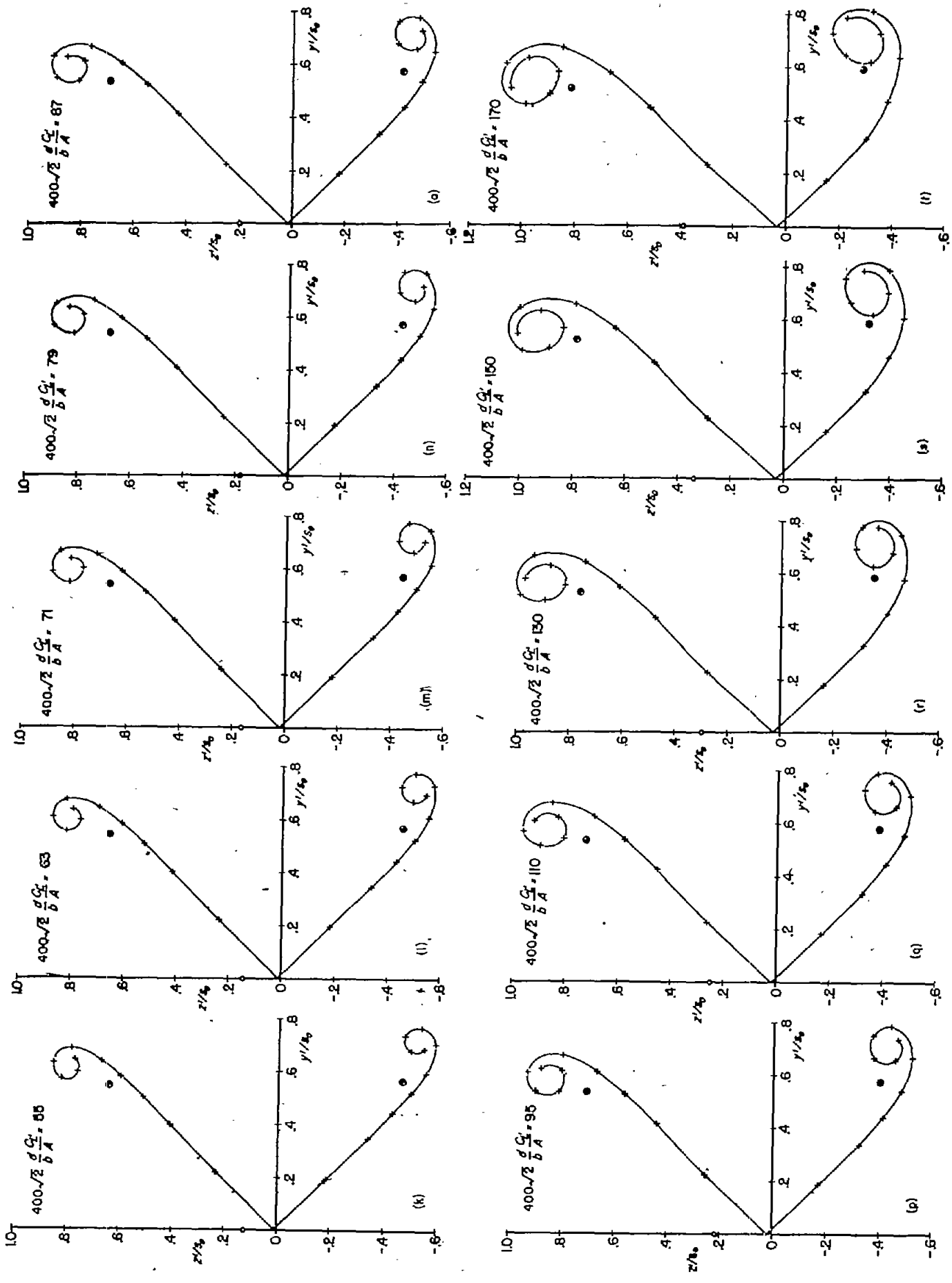

FIGURE 18.—Continued.

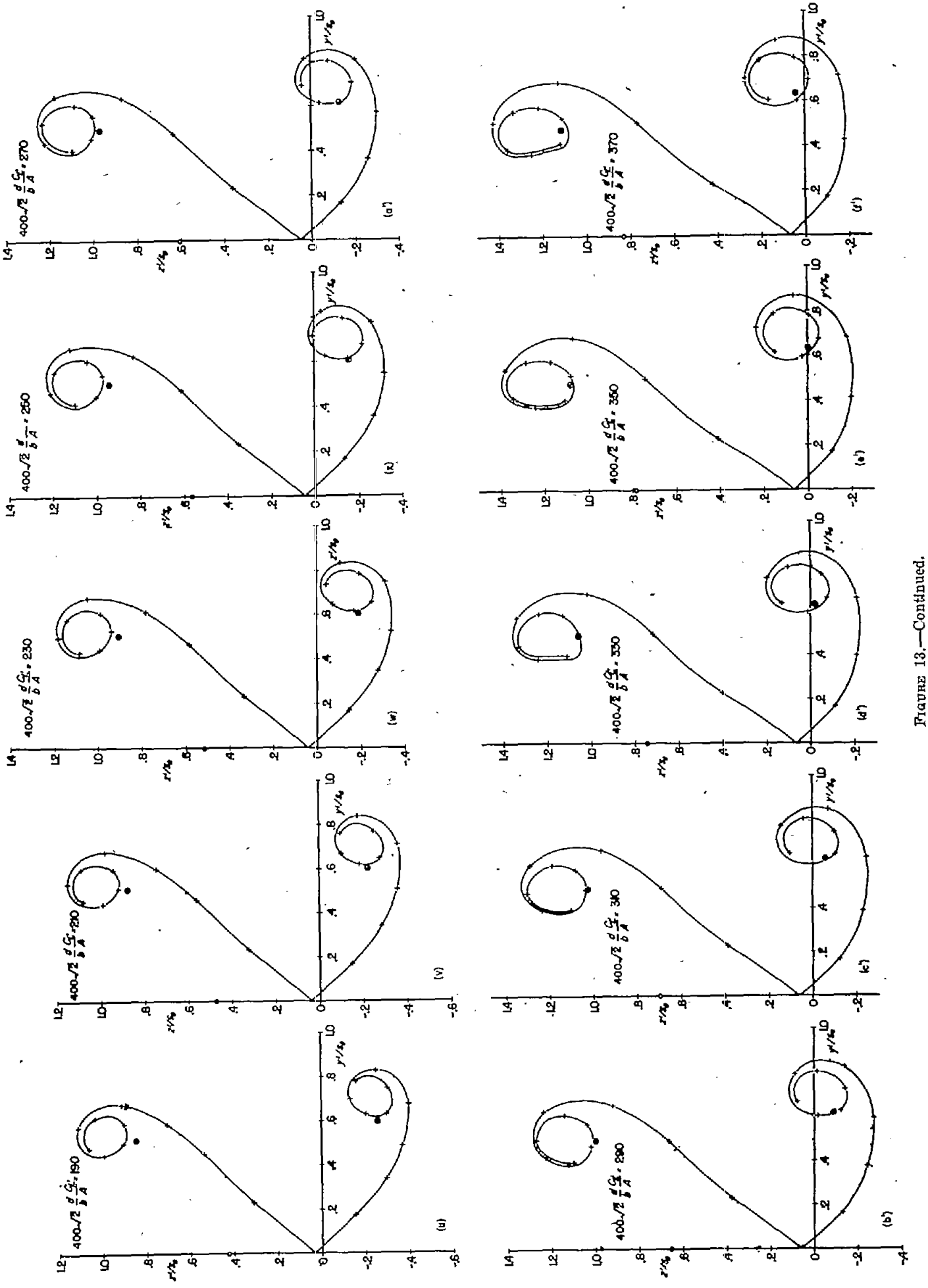

FIGURE 13.—Continued.

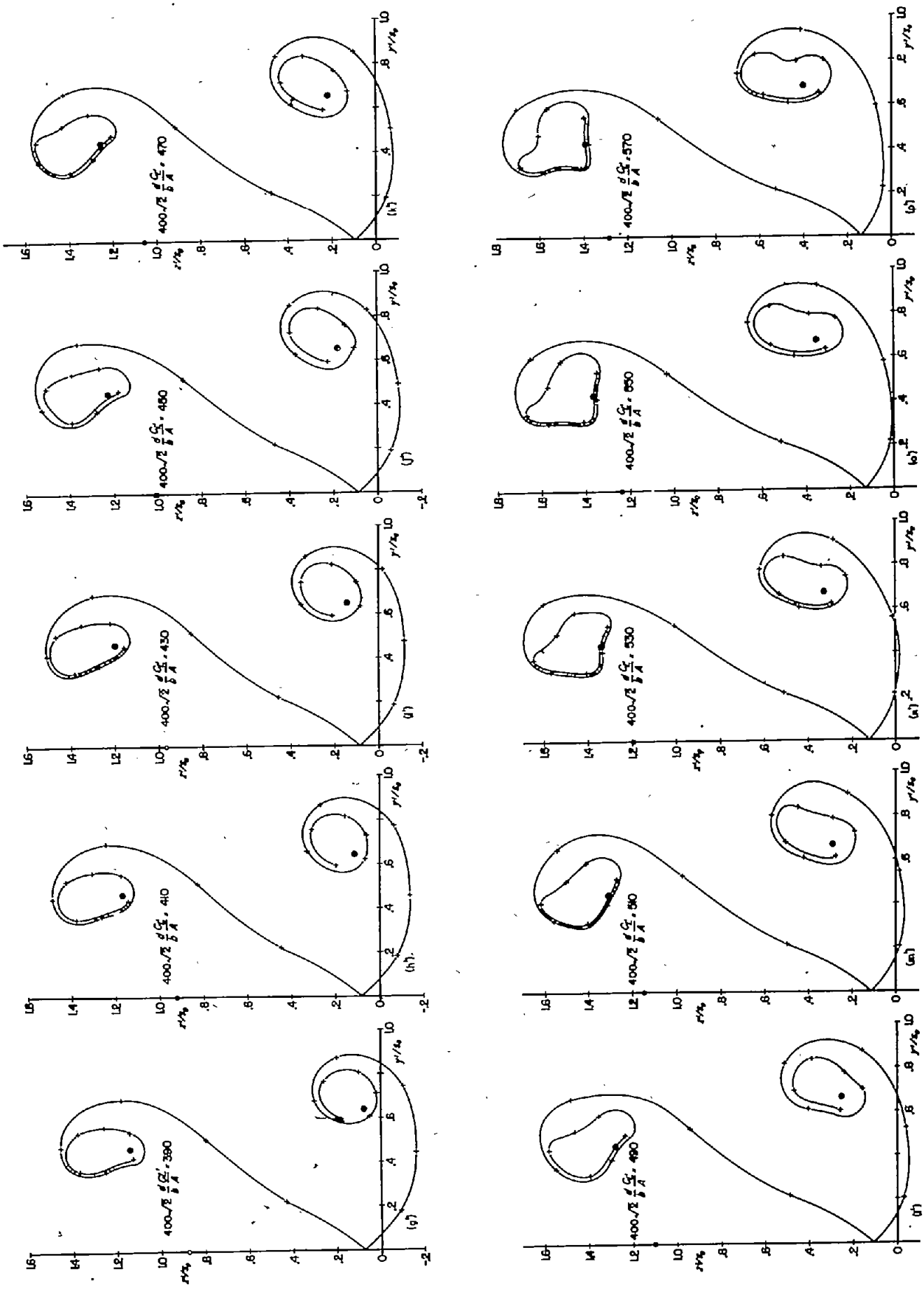

FIGURE 13.—Concluded.

this assumption, which has already been demonstrated for planar wings in reference 1, will be discussed at the end of the present section.

Determination of vortex paths for 45° bank.—In reference 15 an analysis was carried out in which equations were developed for the paths of four rectilinear vortices which start in a symmetrical arrangement as shown in figure 14.[3] In that paper, the analysis was applied to the calculation of the paths of four vortices representing the wake behind an equal-span cruciform wing at 45° bank. It is necessary to reinvestigate this application, however, because the vortex positions at the trailing edge were calculated from the span loading, since it was not recognized that the circulation distribution and span loading were different. The present analysis supersedes the part of reference 15 dealing with the application to the cruciform wing. The results will be given here in terms of the body axes $xy'z'$ defined earlier. From the analysis of reference 15 it is found that if the 4 vortices are of equal strength, the projection of the path of vortex 1 on the $y'z'$ plane is given by (if $G<4$)

$$\frac{z_1'}{f}=\frac{4G}{16-G^2}\left[E(k,\varphi_o)-E(k,\varphi_1)\right]+\frac{G^2}{8(4-G)}\left(\frac{\sin\varphi_1\cos\varphi_1}{\sqrt{1-k^2\sin^2\varphi_1}}-\frac{\sin\varphi_o\cos\varphi_o}{\sqrt{1-k^2\sin^2\varphi_o}}\right)+\frac{1}{8}\sqrt{G(G+4)}\left(\frac{\sin\varphi_1}{\sqrt{1-k^2\sin^2\varphi_1}}-\frac{\sin\varphi_o}{\sqrt{1-k^2\sin^2\varphi_o}}\right)+\frac{y_o'+\alpha' d}{f} \tag{49}$$

where

$$f=y_1'+y_2' \qquad G=\frac{1}{\frac{y_o'}{f}\left(1-\frac{y_o'}{f}\right)}-2$$

y_o'=value of y_1' at wing trailing edge $\qquad k=\frac{G}{4} \qquad d$=distance behind wing trailing edge

$$\sin^2\varphi_o=\frac{R^2-\left(y_o'-\frac{f}{2}\right)^2}{R^2} \qquad \sin^2\varphi_1=\frac{R^2-\left(y_1'-\frac{f}{2}\right)^2}{R^2} \qquad R^2-\frac{f^2G}{4(G+4)}$$

and the subscripts 1 and 2 refer to the vortex numbers indicated in figure 14. The symbol α' represents the angle of attack in the $xy'z'$ coordinate system and is the angle between the x axis and the freestream direction.

The values of y_o', f, and G are to be determined from the spanwise distribution of circulation Γ. For the case of an equal-span triangular cruciform wing banked 45°, the Γ distribution is identical on both component wings and, as shown in equations (34) and (35), is elliptic. Hence, the four vortex lines replacing the vortex sheets are all of equal strength and must be placed at the corners of a square in the plane of the trailing edge. Thus the initial values of y_1' and y_2' must be equal and the lateral position of the centroid of vortices 1 and 2 is given by the average of their y' coordinates. That is,

[3] The motions of 2n vortices were treated by Grobli (Vierteljahrschrift der naturforschenden Gesellschaft in Zurich, vol. 22 (1877), 37-81, 129-167). However, his result for the case of interest here is incorrect.

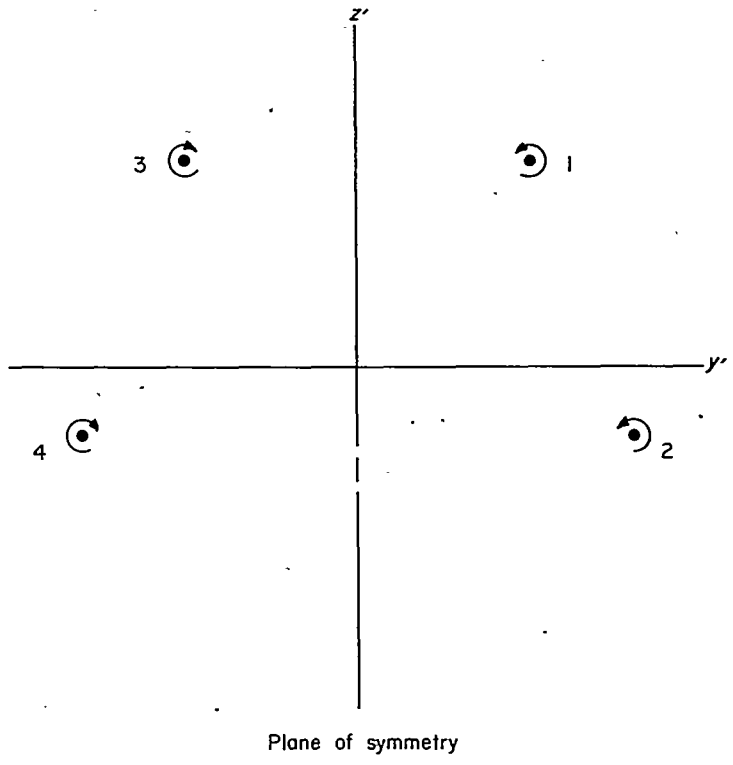

FIGURE 14.—Four vortices in $xy'z'$ system replacing wake behind equal-span cruciform wing at 45° bank.

$$y_c'=\frac{y_1'+y_2'}{2}=\frac{f}{2}=y_o' \tag{50}$$

and therefore $G=2$. Furthermore, since the four vortices are to be placed at the centroids of vorticity from each of the four equal-span panels, one can immediately write, for the elliptic circulation distribution and 45° bank,

$$\frac{y_o'}{s_o}=\frac{\pi}{4\sqrt{2}} \tag{51}$$

Now, since the impulse in the z' direction of the four vortices trailing behind the cruciform wing must be equal to the resultant force in the z' direction, one can write

$$2\rho_\infty U_\infty \Gamma_o f=\frac{1}{2}\rho_\infty U_\infty^2 S C_L' \tag{52}$$

so that

$$\frac{\Gamma_o}{U_\infty s_o}=\frac{C_L'/A}{f/s_o}=\frac{C_L'/A}{2y_o'/s_o}=\frac{2\sqrt{2}}{\pi}\frac{C_L'}{A} \tag{53}$$

where S and A are the area and aspect ratio of one component wing. Thus, all the necessary constants have been obtained for equation (49) so that, upon evaluation of the required elliptic functions, it becomes

$$\frac{z_1'}{f}=\frac{2}{3}\left[1.4675-E\left(\frac{1}{2},\varphi_1\right)\right]+\frac{\sin\varphi_1}{4\sqrt{1-\frac{1}{4}\sin^2\varphi_1}}\left(\cos\varphi_1+\sqrt{3}\right)+\frac{\alpha' d}{f} \tag{54}$$

and it is noted that φ_1 increases positively from its initial value $\varphi_o=\pi/2$ at the wing trailing edge.

In reference 15 it was shown that the path of vortex 2 can be obtained from that of vortex 1 by the use of the expression for the relative paths

$$\left(\frac{z_1'-z_2'}{f}\right)^2=\frac{G\frac{y_1'}{f}\left(1-\frac{y_1'}{f}\right)-\left(2\frac{y_1'}{f}-1\right)^2}{1-G\frac{y_1'}{f}\left(1-\frac{y_1'}{f}\right)} \tag{55}$$

so that (since $G=2$)

$$\left(\frac{z_1'-z_2'}{f}\right)^2=\frac{6\frac{y_1'}{f}-6\left(\frac{y_1'}{f}\right)^2-1}{2\left(\frac{y_1'}{f}\right)^2-2\frac{y_1'}{f}+1} \tag{56}$$

Similarly, with the use of equations (50) to (53), the expression given in reference 15 for distance behind the wing

$$\frac{d}{f}=\frac{\pi U_\infty f}{\Gamma_o}\left\{-\frac{128}{G(16-G^2)}\left[E(k,\varphi_o)-E(k,\varphi_1)\right]+\frac{8}{G}\left[F(k,\varphi_o)-F(k,\varphi_1)\right]+\frac{G}{4-G}\left(\frac{\sin\varphi_o\cos\varphi_o}{\sqrt{1-k^2\sin^2\varphi_o}}-\frac{\sin\varphi_1\cos\varphi_1}{\sqrt{1-k^2\sin^2\varphi_1}}\right)\right\} \tag{57}$$

reduces to

$$\frac{d}{f}=\frac{\pi^3}{8}\frac{A}{C_L'}\left[-1.0834+\frac{16}{3}E\left(\frac{1}{2},\varphi_1\right)-4F\left(\frac{1}{2},\varphi_1\right)-\frac{\sin\varphi_1\cos\varphi_1}{\sqrt{1-\frac{1}{4}\sin^2\varphi_1}}\right] \tag{58}$$

so that the paths of vortices 1 and 2 are completely defined by equations (50), (54), (56), and (58) and the paths of vortices 3 and 4 are found by symmetry. The leapfrog distance, which is defined by the condition $z_1'=z_2'$, is obtained by setting $\varphi_1=\pi$. The last term in the bracketed expression above then vanishes and the distance d_L can be expressed, after evaluation of the necessary elliptic functions, as

$$\frac{d_L}{f}=\frac{\pi^3}{8}\frac{A}{C_L'}(1.0834) \tag{59}$$

$$\frac{d_L}{b}=\frac{d_L f}{f b}=2.332\frac{A}{C_L'}=\frac{4.664}{\pi\alpha'} \tag{60}$$

Note that this relation has exactly the form of equation (41) and is independent of plan form.

Comparison with results of 40-vortex calculation.—It is evident that at very large distances behind the wing the centroids of the vorticity shed from each panel must lie within the rolled-up vortex cores. Hence, the problem of determining the positions of the rolled-up vortices is essentially that of determining the positions of the centroids of vorticity at distances greater than the rolling-up distance behind the wing. If this is to be done by using four vortex lines leaving the trailing edge at the centroid-of-vorticity positions, then the assumption must be made that the positions of the four vortices as determined by equations (50), (54), (56), and (58) coincide with the positions of the centroids of vorticity at all distances behind the wing. This assumption has therefore been made in the above analysis. In order to investigate the validity of this assumption for 45° bank, comparisons have been made at various distances behind the wing between the vortex positions given by the present 4-vortex analysis and the centroid-of-vorticity positions obtained from the 40-vortex numerical calculations of the preceding section. The latter positions were calculated according to the relations

$$y_c'=\frac{\Sigma y_t'\Gamma_t}{\Sigma\Gamma_t};\qquad z_c'=\frac{\Sigma z_t'\Gamma_t}{\Sigma\Gamma_t} \tag{61}$$

for the vortex sheet from each wing panel, and these positions are tabulated in table II and indicated on the plots of figure 13 by the symbol customarily used for the center-of-gravity position. The fact that the centroid-of-vorticity positions become indicative of the vortex-core positions only after the vortex cores are well developed is clearly illustrated by the centroid-of-vorticity positions of figure 13. On the other hand, the comparison shown in figure 15 of the centroid-of-vorticity positions for the 4- and the 40-vortex approximations indicates that the agreement is remarkably good for all distances behind the wing. It can therefore be concluded that the vortex positions obtained in the present 4-vortex analysis furnish good approximations to the positions of the vortex cores at distances behind the wing at which the rolling-up process is essentially completed.

Determination of initial slopes of vortex paths for all bank angles.—The analytical method of the present section is restricted to an angle of bank of 45° inasmuch as a solution was obtained by making use of symmetry considerations. For other angles of bank, it is doubtful that a closed analytical solution could be obtained for the paths of even the simple 4-vortex model. It is a simple matter, however, to write analytical expressions for the initial slopes of the 4 vortex lines at the wing trailing edge; and it is possible to write corresponding expressions for the initial slopes of the paths described by the centroids of vorticity of the flat vortex sheets leaving the trailing edge. In this way, one can gain some idea of whether the 4-vortex approximation might be a good one for other angles of bank. It will be convenient here to return to the xyz body axes lying in the planes of the wing panels. In this coordinate system it becomes clear that the y and z components of the slopes of the vortices from opposing panels are equal. Thus, equations (31) through (33) reduce for the 4-vortex model to

$$\left.\begin{aligned}\left(\frac{dy_1}{dx}\right)_{d=0}&=\left(\frac{dy_4}{dx}\right)_{d=0}=-\beta+\frac{\Gamma_{o_V}}{\pi^2U_\infty t_o}\\ \left(\frac{dz_1}{dx}\right)_{d=0}&=\left(\frac{dz_4}{dx}\right)_{d=0}=\alpha-\frac{4\Gamma_{o_H}s_o}{\pi^2U_\infty(s_o^2+t_o^2)}\\ \left(\frac{dy_2}{dx}\right)_{d=0}&=\left(\frac{dy_3}{dx}\right)_{d=0}=-\beta+\frac{4\Gamma_{o_V}t_o}{\pi^2U_\infty(s_o^2+t_o^2)}\\ \left(\frac{dz_2}{dx}\right)_{d=0}&=\left(\frac{dz_3}{dx}\right)_{d=0}=\alpha-\frac{\Gamma_{o_H}}{\pi^2U_\infty s_o}\end{aligned}\right\} \tag{62}$$

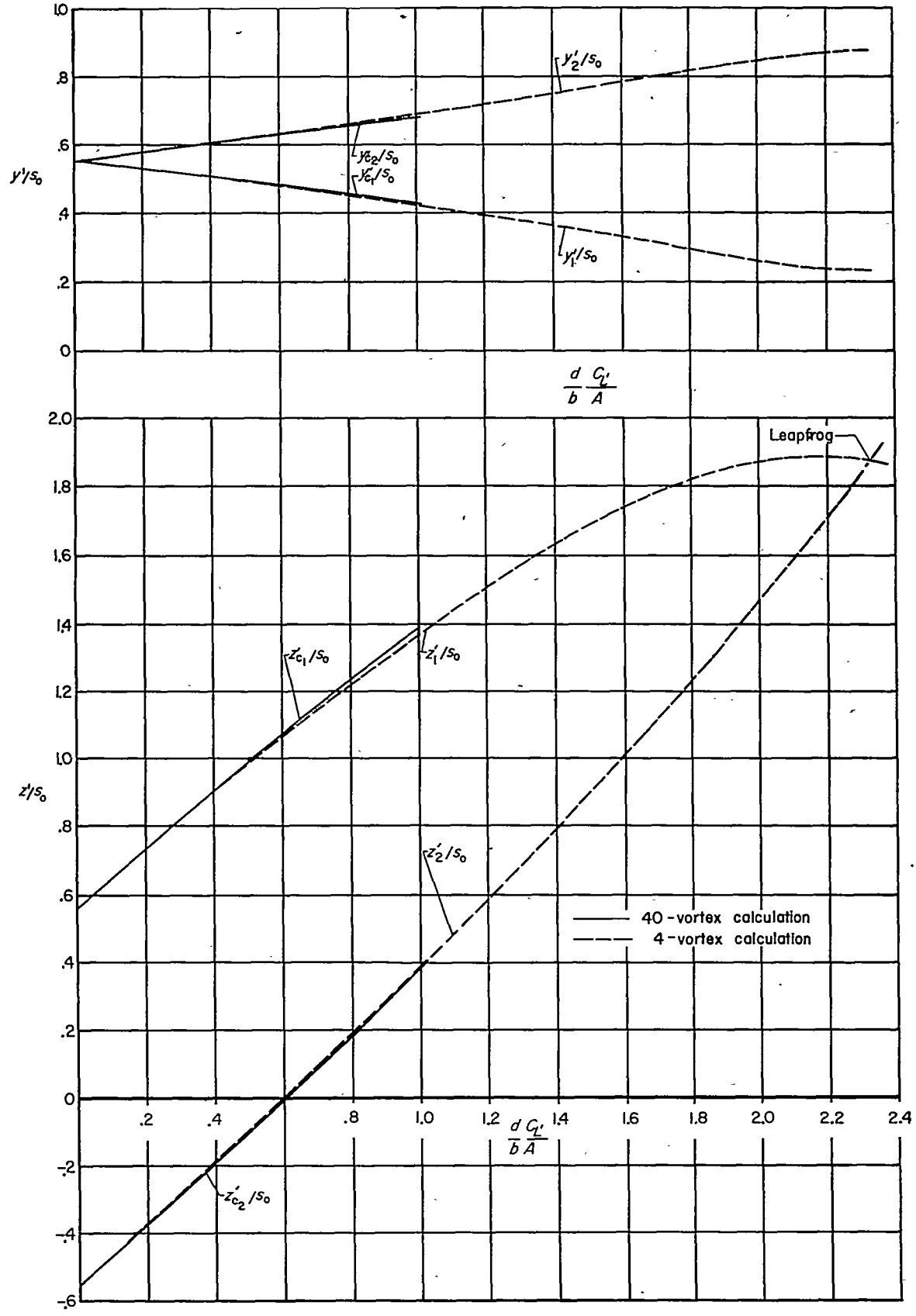

FIGURE 15.—Comparison of positions of centroids of vorticity calculated with 4 and with 40 discrete vortices.

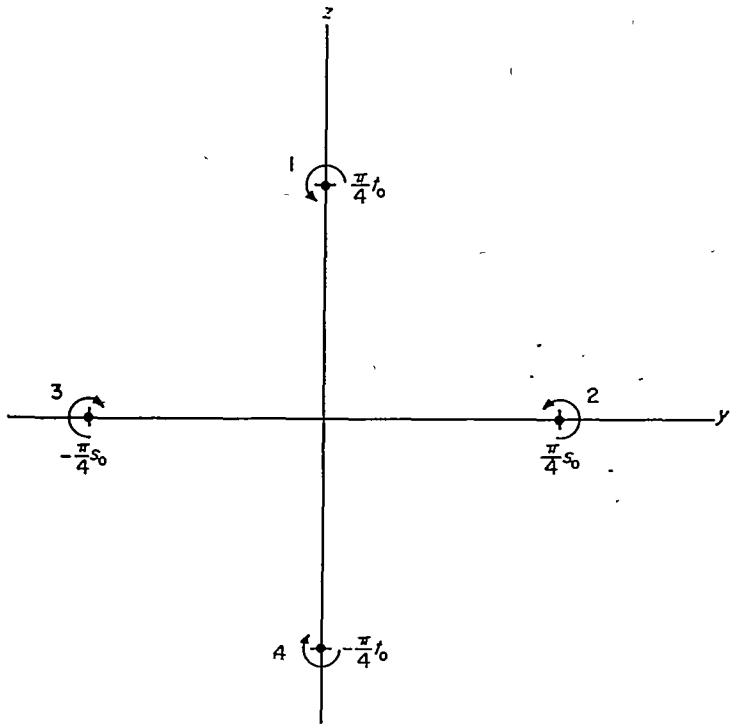

FIGURE 16.—Initial positions of four vortices in xyz coordinate system.

where the subscripts 1 through 4 refer to the vortices numbered as shown in figure 16, and Γ_{o_H} and Γ_{o_H} refer to the maximum circulations of the horizontal- and vertical-wing components, respectively. Since the latter quantities are related to the angle of attack and the angle of sideslip according to

$$\alpha=\frac{\Gamma_{o_H}}{2U_\infty s_o};\ \beta=\frac{\Gamma_{o_H}}{2U_\infty t_o} \tag{63}$$

the expressions of equation (62) can be rewritten as follows:

$$\left.\begin{aligned}
\left(\frac{dy_1}{dx}\right)_{d=0}&=\left(\frac{dy_4}{dx}\right)_{d=0}=\beta\left(-1+\frac{2}{\pi^2}\right)\\
\left(\frac{dz_1}{dx}\right)_{d=0}&=\left(\frac{dz_4}{dx}\right)_{d=0}=\alpha\left[1-\frac{8}{\pi^2\left(1+\frac{t_o^2}{s_o^2}\right)}\right]\\
\left(\frac{dy_2}{dx}\right)_{d=0}&=\left(\frac{dy_3}{dx}\right)_{d=0}=\beta\left[-1+\frac{8}{\pi^2\left(1+\frac{s_o^2}{t_o^2}\right)}\right]\\
\left(\frac{dz_2}{dx}\right)_{d=0}&=\left(\frac{dz_3}{dx}\right)_{d=0}=\alpha\left(1-\frac{2}{\pi^2}\right)
\end{aligned}\right\} \tag{64}$$

Determination of initial slopes of centroids of vorticity of the vortex sheets for all bank angles.—For comparison with the above 4-vortex approximation, consider now the initial slopes of the paths described by the centroids of the vorticity trailing from each panel of the cruciform wing. Inasmuch as the singularities at the edges of the wake contribute substantially to the slopes of these paths, and conditions in the immediate vicinity of such singularities are difficult to investigate directly, a control-surface type of analysis will be used. As will become evident on reading, the analysis bears many features of resemblance to that employed in the calculation of forces on the leading edges of thin wings. To start, consider that portion of the trailing-vortex system contained between two parallel planes normal to the x axis and dx apart, and inside an arbitrary cylindrical surface C having generators parallel to the x axis, as illustrated in figure 17. The y and z coordinates of the centroid of vorticity of the enclosed portion of the vortex system are given by

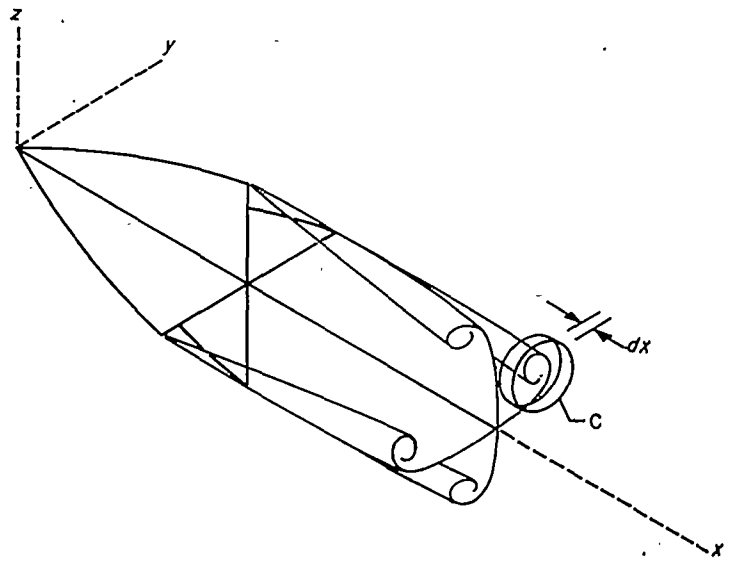

FIGURE 17.—Vortex wake and cylindrical control surface C.

$$y_c=\frac{\Sigma y_t\Gamma_t}{\Sigma\Gamma_t};\qquad z_c=\frac{\Sigma z_t\Gamma_t}{\Sigma\Gamma_t} \tag{65}$$

where y_t and z_t are the coordinates of a vortex having strength Γ_t, and the summations are extended over all vortices extending through the planar ends of the control surface. Since the slopes of each vortex filament are given, according to equations (31) through (33), by

$$\frac{dy_t}{dx}=\frac{v_{t_u}+v_{t_l}}{2U_\infty}=\frac{\overline{v}_t}{U_\infty};\qquad \frac{dz_t}{dx}=\frac{w_{t_u}+w_{t_l}}{2U_\infty}=\frac{\overline{w}_t}{U_\infty} \tag{66}$$

the slopes of the path of the centroid of vorticity are

$$\frac{dy_c}{dx}=\frac{\Sigma\overline{v}_t\Gamma_t}{U_\infty\Sigma\Gamma_t};\qquad \frac{dz_c}{dx}=\frac{\Sigma\overline{w}_t\Gamma_t}{U_\infty\Sigma\Gamma_t} \tag{67}$$

Now, an important consequence of the fact that the flow in the vicinity of the wake is governed by Laplace's equation, that is, by equation (5), is that the velocities at any station are the same whether the vortices at that station are free or fixed. This means that

$$v_{t_{free}}=v_{t_{fixed}}=v_t;\ w_{t_{free}}=w_{t_{fixed}}=w_t \tag{68}$$

In contrast to the force-free state of the actual trailing-vortex system, the fixed-vortex system sustains forces given by

$$dY_t=-\rho_\infty\overline{w}_t\Gamma_t dx;\qquad dL_t=\rho_\infty\overline{v}_t\Gamma_t dx \tag{69}$$

on each vortex filament, or

$$\left.\begin{aligned}
dY&=\Sigma dY_t=-\rho_\infty\Sigma\overline{w}_t\Gamma_t dx\\
dL&=\Sigma dL_t=\rho_\infty\Sigma\overline{v}_t\Gamma_t dx
\end{aligned}\right\} \tag{70}$$

in total. Combining equations (67) and (70) yields the following relations:

$$\frac{dy_c}{dx}=\frac{dL}{\rho_\infty U_\infty \Sigma\Gamma_i dx};\qquad \frac{dz_c}{dx}=-\frac{dY}{\rho_\infty U_\infty \Sigma\Gamma_i dx} \tag{71}$$

Hence, the slopes of the lines connecting the centroid-of-vorticity positions of the free-vortex system can be determined from the forces on the fixed-vortex system.

The total forces dY and dL on the fixed system can be determined by applying momentum methods to the control surface shown in figure 17. This calculation is simplified by the fact that the pressures and flow of momentum through the plane faces exactly counterbalance, leaving only the contributions from the contour C. Thus

$$\left.\begin{aligned}\frac{dY}{dx}&=-\int_C p\,dz-\rho_\infty\int_C v(v\,dz-w\,dy)\\ \frac{dL}{dx}&=\int_C p\,dy+\rho_\infty\int_C w(w\,dy-v\,dz)\end{aligned}\right\} \tag{72}$$

where the integrals are to be taken in the counterclockwise sense and the pressure p is related to the velocity components according to equations (10), (31), and (32), that is

$$\left.\begin{aligned}p&=p_\infty-\rho_\infty U_\infty(\varphi_x+\alpha\varphi_z-\beta\varphi_y)-\frac{\rho_\infty}{2}(\varphi_y^2+\varphi_z^2)\\ &=p_\infty-\rho_\infty U'_\infty\varphi_x+\frac{\rho_\infty}{2}U_\infty^2(\alpha^2+\beta^2)-\frac{\rho_\infty}{2}(v^2+w^2)\end{aligned}\right\} \tag{73}$$

Now, p_∞, α, and β are constants and contribute nothing to the integral of equation (72) when integrated around the contour, and φ_x is zero because the vortices are fixed. Hence, equation (72) can be rewritten as follows:

$$\left.\begin{aligned}\frac{dY}{dx}&=\frac{\rho_\infty}{2}\int_C[(w^2-v^2)dz+2vw\,dy]\\ \frac{dL}{dx}&=\frac{\rho_\infty}{2}\int_C[(w^2-v^2)dy-2vw\,dz]\end{aligned}\right\} \tag{74}$$

Finally, on substitution of equation (74) into equation (71), we have the following relations between the slopes of the path of the centroid of vorticity and the velocity components v and w which exist at the location of the cylindrical control surface C.

$$\left.\begin{aligned}\frac{dy_c}{dx}&=\frac{1}{U_\infty\Sigma\Gamma_i}\int_C\left[-vw\,dz+\frac{(-v^2+w^2)}{2}dy\right]\\ \frac{dz_c}{dx}&=-\frac{1}{U_\infty\Sigma\Gamma_i}\int_C\left[vw\,dy+\frac{(-v^2+w^2)}{2}dz\right]\end{aligned}\right\} \tag{75}$$

where

$$\Sigma\Gamma_i=-\int_C(v\,dy+w\,dz) \tag{76}$$

The above results will now be applied to the calculation of the initial slopes of the path of the centroid of the vorticity trailing from the wing panel which extends along the positive y axis. In keeping with the notation of figure 16, this panel will be designated with the number 2. If the control surface C is selected as shown in figure 18, the integrals of equations (75) and (76) can be divided into three parts.

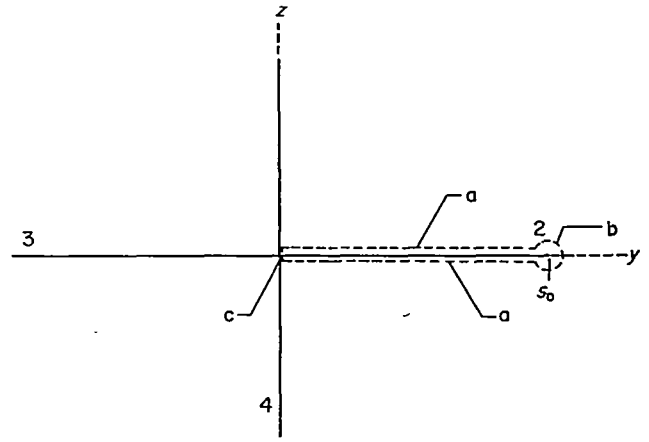

FIGURE 18.—Components of selected control surface.

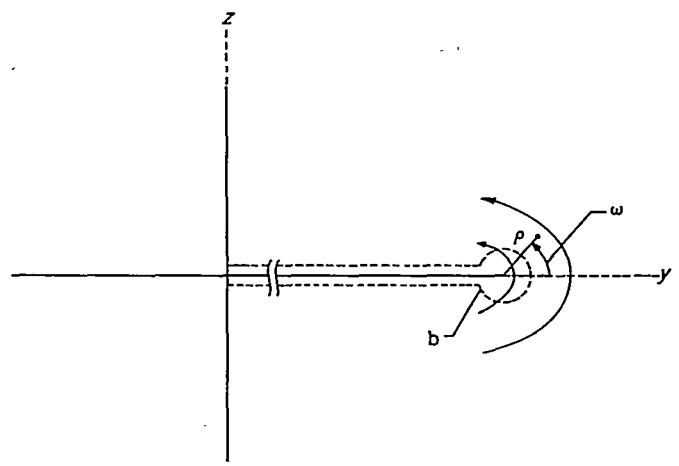

FIGURE 19.—Polar coordinates near edge of wake.

The contributions of part a can be written directly, and that of part b can be evaluated by considering the asymptotic form of the velocities in the vicinity of the edge of the wake to be the same as that of the velocities around the edge of a flat plate; that is,

$$v=-\frac{\mu}{\sqrt{\rho}}\sin\frac{\omega}{2};\quad w=\frac{\mu}{\sqrt{\rho}}\cos\frac{\omega}{2} \tag{77}$$

where ρ and ω are polar coordinates, with origin at the edge of the wake as indicated in figure 19, and μ is a constant. The contribution of part c is zero because dy is zero, dz approaches zero, and the velocities are nonsingular there. Upon carrying out the necessary operations, one finds that the slopes of the path of the centroid of vorticity immediately behind the wing are

$$\left.\begin{aligned}\left(\frac{dy_{c_2}}{dx}\right)_{d=0}&=-\frac{1}{U_\infty\Gamma_{o_H}}\int_0^{s_0}\bar{v}\frac{d\Gamma}{dy}dy\\ \left(\frac{dz_{c_2}}{dx}\right)_{d=0}&=\frac{1}{U_\infty\Gamma_{o_H}}\left[\int_0^{s_0}-w\frac{d\Gamma}{dy}dy+\mu^2\pi\right]\end{aligned}\right\} \tag{78}$$

The velocity components v and w can in turn be expressed in terms of the circulation distribution at the trailing edge by employing equations (31) and (32). The circulation distributions on both the horizontal- and vertical-wing com-

ponents are elliptic, according to equations (34) and (35). Hence,

$$\Gamma_{o_H}=2U_\infty \alpha s_o;\ \Gamma_{o_V}=2U_\infty \beta t_o \tag{79}$$

It also follows from equations (76) and (77) that

$$\mu=U_\infty \alpha \sqrt{\frac{s_o}{2}} \tag{80}$$

and therefore

$$\left.\begin{aligned}\left(\frac{dy_{c2}}{dx}\right)_{d=0}&=-\beta\sqrt{1+\frac{t_o^2}{s_o^2}}\left[E\left(\sin^{-1}\frac{1}{\sqrt{1+\frac{t_o^2}{s_o^2}}}\right)-\frac{t_o^2/s_o^2}{1+\frac{t_o^2}{s_o^2}}K\left(\sin^{-1}\frac{1}{\sqrt{1+\frac{t_o^2}{s_o^2}}}\right)\right]\\ \left(\frac{dz_{c2}}{dx}\right)_{d=0}&=\frac{\pi}{4}\alpha\end{aligned}\right\} \tag{81}$$

For cruciform wings having horizontal and vertical components of equal span, that is, $s_o=t_o$, the relations of equation (81) reduce to

$$\left(\frac{dy_{c2}}{dx}\right)_{d=0}=-0.599\beta;\left(\frac{dz_{c2}}{dx}\right)_{d=0}=0.785\alpha \tag{82}$$

These results also apply to the initial slopes of the path of the centroid of the vorticity trailing from panel 3. The corresponding expressions for panel 1, and likewise panel 4, can be found by the proper interchange of quantities and are

$$\left(\frac{dy_{c1}}{dx}\right)_{d=0}=-0.785\beta;\left(\frac{dz_{c1}}{dx}\right)_{d=0}=0.599\alpha \tag{83}$$

These results may be compared with the corresponding values for the inital slopes of the vortex lines of the 4-vortex approximation to the wake of an equal-span cruciform wing by substituting $s_o=t_o$ into the relations of equation (64).

$$\left(\frac{dy_1}{dx}\right)_{d=0}=-0.797\beta;\left(\frac{dz_1}{dx}\right)_{d=0}=0.595\alpha \tag{84}$$

$$\left(\frac{dy_2}{dx}\right)_{d=0}=-0.595\beta;\left(\frac{dz_2}{dx}\right)_{d=0}=0.797\alpha \tag{85}$$

It can be seen by comparing the results of the immediately preceding equations that the initial slopes of the individual vortex lines of the 4-vortex model are very nearly the same as the initial slopes of the paths of the centroids of vorticity of the corresponding portions of the continuous vortex sheet. This conclusion serves as a first indication that the 4-vortex model may be as satisfactory for determining the positions of the rolled-up vortex cores at great distances from the wing for all angles of bank as was demonstrated for 45° bank in figures 13 and 15.

WATER-TANK EXPERIMENTS

Experiments were conducted in a water tank for the purpose of observing visually the vortex paths calculated in the foregoing analysis. Photographs were obtained of the wake at various distances behind a cruciform wing by plunging a model vertically into the water at uniform speed and photographing the water surface from above with a moving-picture camera. The traces of the wake were made visible by applying fine aluminum powder to the wing trailing edges. The models tested were triangular flatplate wings of aspect ratio 2.

Abridged series of photographs are presented for angles of bank of 0° (plane wing) and 45° in figures 20 and 21, respectively. The latter results are shown for distances up to the leapfrog distance d_L behind the wing, and measurements of this distance were obtained by means of a tape which moved with the model and recorded on the film the distance between the wing trailing edge and the water surface. The results of such observations at various angles of attack are presented in figure 22 and compared with the 4-vortex calculation of equation (60). The agreement is seen to be quite satisfactory except possibly at the very high lift coefficients. The lift coefficients for the experimental points were calculated from equation (48).

Because of the persistence of the vortex sheets connecting the vortex cores (see figs. 13 and 20), the 4-vortex approximation may not yield accurate vortex paths at distances behind the wing greater than about d_L since the sheets may upset the periodic nature of the predicted paths. The 4-vortex approximation likewise cannot be expected to give the vortex core positions accurately at distances behind the wing at which the vortex sheets are only partially rolled up since there the positions of the centroids of vorticity do not correspond to the vortex cores, as discussed previously in connection with figure 13.

LIFT ON A TAIL IN A NONUNIFORM DOWNWASH FIELD

Once the vortex positions at the tail station are known through calculations similar to those described in the preceding sections, or by other means, the associated downwash and sidewash fields and the lift and side force on the tail can be determined by direct calculation. The determination of the lateral velocities can be accomplished by substituting the known strengths and positions of the vortices into equations (31) and (32) and integrating (or summing in the case of a discrete vortex approximation). This problem is exactly the same as the classical problem of determining the incompressible flow field associated with a distribution of rectilinear vortices, and several alternative methods are available for obtaining the solution.

The determination of the lift and side force on a tail in a nonuniform downwash field of known structure is the remaining task necessary to complete the calculation of such quantities as the lift and center of pressure of a wing-tail system. Although the solution of this problem is often approximated by the introduction of additional assumptions

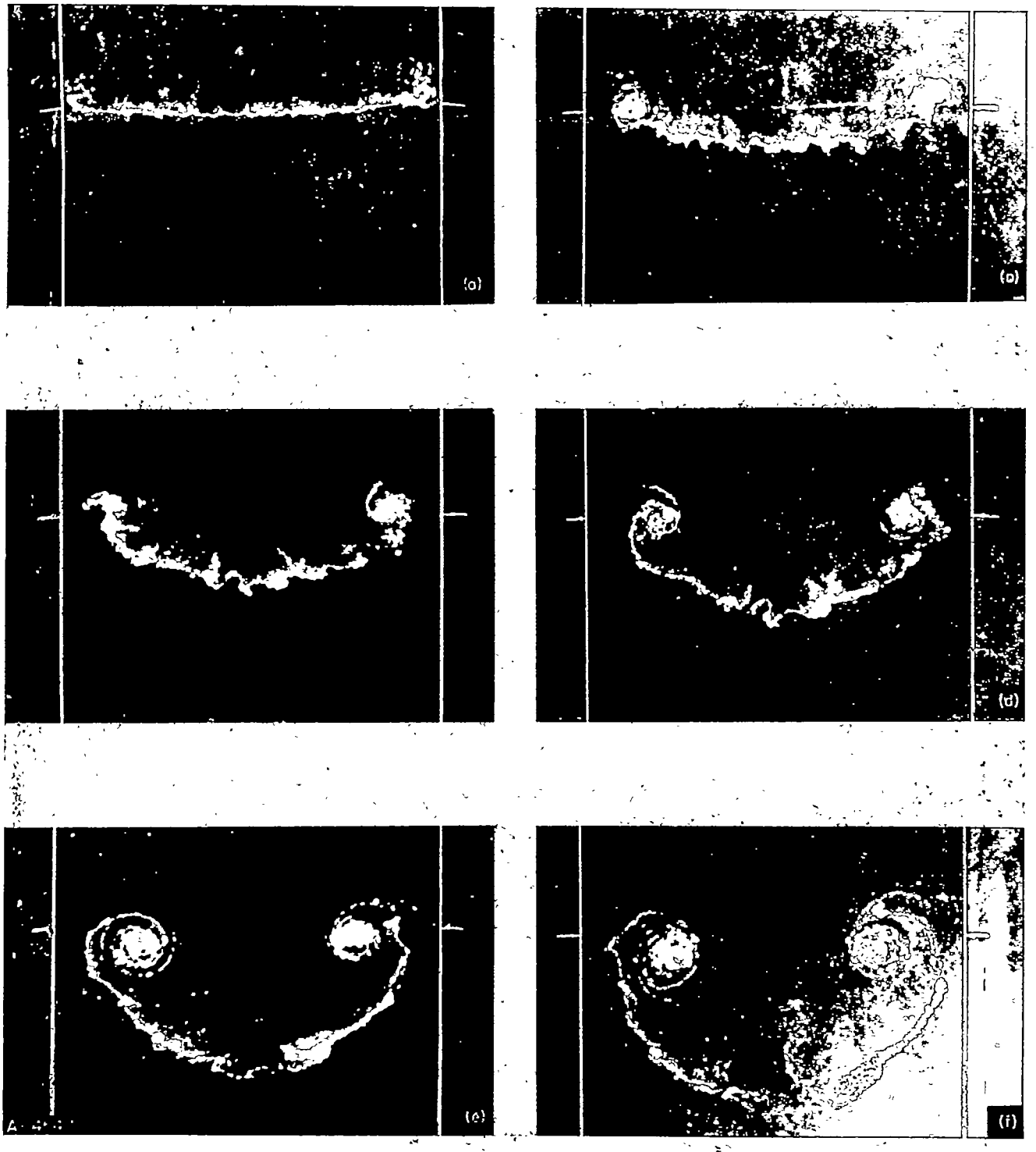

(a) $d/b=0.09$.
(b) $d/b=0.35$.
(c) $d/b=0.60$.
(d) $d/b=0.89$.
(e) $d/b=1.45$.
(f) $d/b=1.80$.

FIGURE 20.—Photographs of the wake at various distances behind a triangular plane wing (or cruciform wing at $\phi=0$) of aspect ratio, 2; $\alpha=20°$.

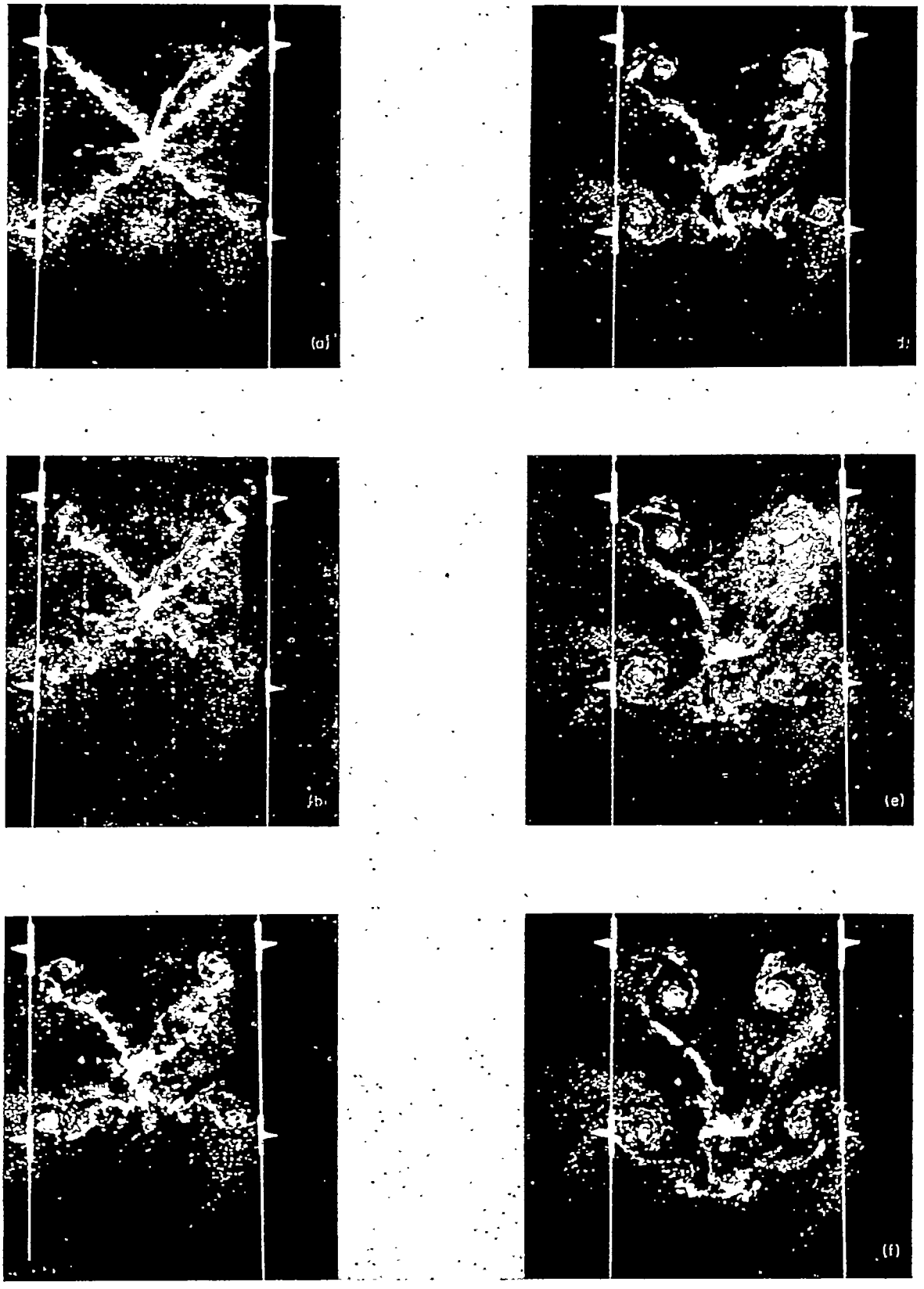

(a) $d/b=0.11$.
(b) $d/b=0.33$.
(c) $d/b=0.61$.
(d) $d/b=0.94$.
(e) $d/b=1.38$.
(f) $d/b=1.79$.

FIGURE 21.—Photographs of the wake at various distances behind an equal-span triangular cruciform wing of aspect ratio 2; $\phi=45°$, $\alpha'=17°$.

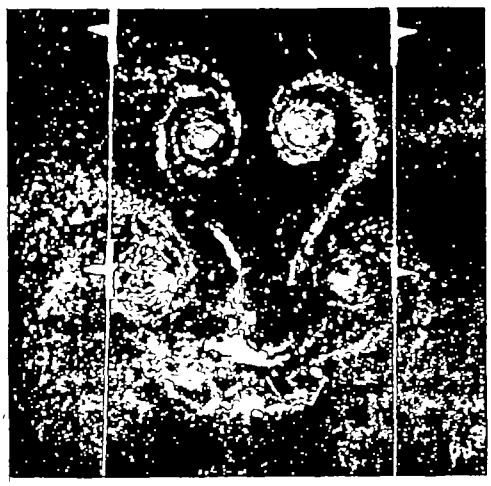

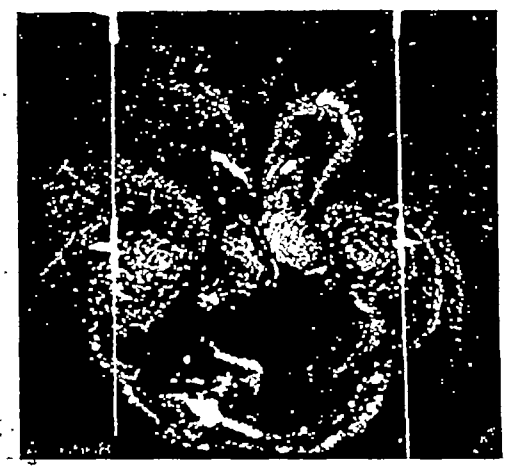

(g) $d/b=2.24$.
(h) $d/b=2.83$.
(i) $d/b=3.65$.
(j) $d/b=4.26$.
(k) $d/b=4.81$.

FIGURE 21.—Concluded.

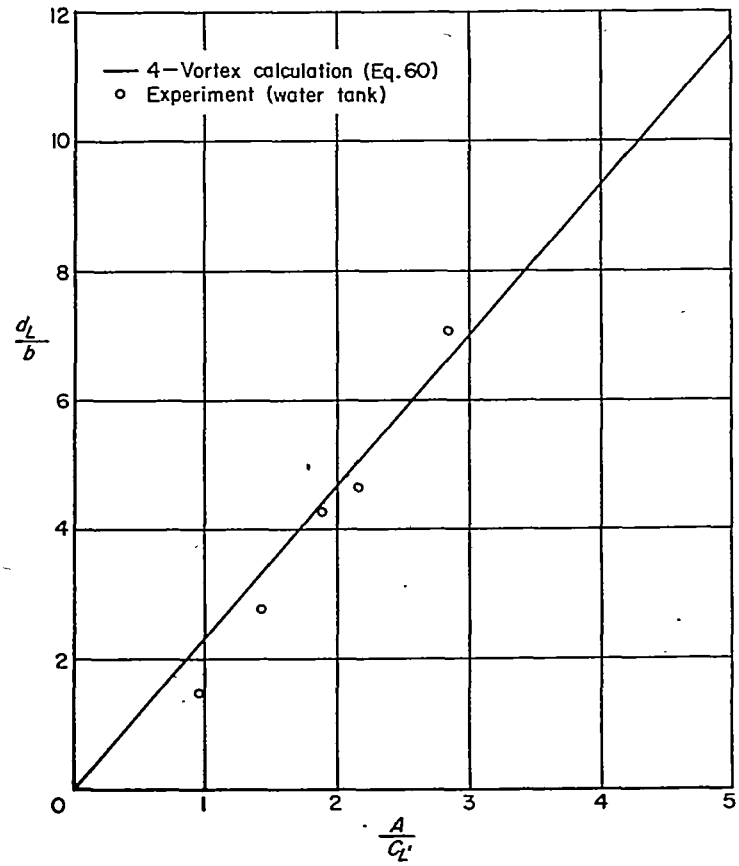

FIGURE 22.—Comparison of theory and experiment for leapfrog distance behind equal-span cruciform wing ($\phi=45°$).

such as strip theory, etc., the exact linear-theory solution can be obtained by use of reciprocal theorems. This has already been demonstrated in reference 16 and elsewhere for the case where the tail is a planar surface of sufficiently high aspect ratio that the linear pressure-velocity relation can be used. The following discussion will be concerned with the derivation of the corresponding relationship that is consistent with the formulation of slender-body theory summarized in the first section of the present analysis for the lift of a low-aspect-ratio cruciform wing having flat-plate wing panels. This aim will be accomplished by considering certain properties associated with a second cruciform wing identical to the first, but immersed in a uniform flow field streaming in the opposite direction to that about the first wing, as illustrated in figure 23. Inasmuch as wing 1 is immersed in a nonuniform flow field, the local or effective angles of attack and sideslip $\tilde{\alpha}$ and $\tilde{\beta}$ are variable, that is

$$\left.\begin{aligned}\tilde{\alpha}_1(x,y)&=\frac{w_1}{U_\infty}=\alpha_1+\frac{(\varphi_z)_1}{U_\infty}\\ \tilde{\beta}_1(x,z)&=-\frac{v_1}{U_\infty}=\beta_1-\frac{(\varphi_y)_1}{U_\infty}\end{aligned}\right\} \tag{86}$$

where α_1 and β_1 represent the geometric angles of attack and sideslip, and $(\varphi_y)_1$ and $(\varphi_z)_1$ represent the additional lateral velocity components induced, say, by the vortex system trailing from a wing somewhere upstream. In order to express the lift on wing 1 in terms of simple properties of the flow about wing 2, it is necessary that wing 2 be at zero sideslip, thus

$$\beta_2=0 \tag{87}$$

The proper reciprocal relation for use with multiplanar systems is given in reference 16 and is

$$\iint_\Sigma u_1(V_n)_2 dS=\iint_\Sigma u_2(V_n)_1 dS \tag{88}$$

where the area of the integration Σ extends over both sides of all wing surfaces, V_n is the component of the perturbation velocity normal to and directed away from the surface, and the subscripts 1 and 2 refer to conditions on wings 1 and 2. Since, for wings having no thickness, V_n is equal and opposite on the two sides of its surface, and is furthermore proportional to $\tilde{\alpha}$ on wing component H and to $\tilde{\beta}$ on wing component V, equation (88) can be rewritten as follows:

$$\iint_H \Delta u_1 \tilde{\alpha}_2 dx\,dy+\iint_V \Delta u_1 \tilde{\beta}_2 dx\,dz = \iint_H \Delta u_2 \tilde{\alpha}_1 dx\,dy+\iint_V \Delta u_2 \tilde{\beta}_1 dx\,dz \tag{89}$$

Here Δu refers to the difference in u on the two sides of any surface and the subscripts H and V indicate that the inte-

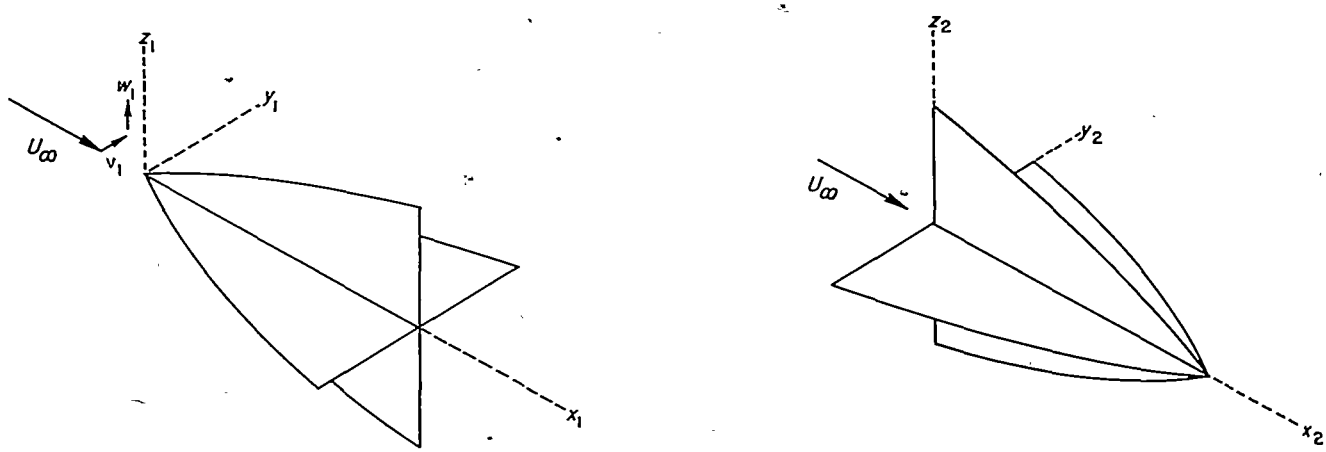

FIGURE 23.—Cruciform wing in forward and reverse flow.

grals are to be carried over wings H and V, respectively. In the present case, simplification occurs not only because $\tilde{\alpha}_2$=const., and $\tilde{\beta}_2=0$, but also because it follows therefrom that $\Delta u_2=0$ on wing V. Thus equation (89) reduces to

$$\tilde{\alpha}_2 \iint_H \Delta u_1 dS = \iint_H \Delta u_2 \tilde{\alpha}_1 dS \tag{90}$$

Now if the integral on the left side of equation (90) is rewritten in terms of φ and integrated with respect to x, that is

$$\iint_H \Delta u_1 dS = \iint_H \Delta \frac{\partial \varphi_1}{\partial x} dx\, dy = \int_{-s_o}^{+s_o} (\Delta\varphi_1)_{TE} dy \tag{91}$$

where the subscript TE refers to the values of $\Delta\varphi_1$ at the trailing edge, and if equation (26) is recalled for the lift including the effects of the nonlinear terms in the pressure-velocity relation of equation (10),

$$L=\rho_\infty U_\infty \int_{-s_o}^{+s_o} \Delta\varphi_{TE} dy \tag{26}$$

equation (90) becomes

$$L_1=\rho_\infty U_\infty \iint_H \left(\frac{\Delta u_2}{\tilde{\alpha}_2}\right)\tilde{\alpha}_1 dx\, dy \tag{92}$$

In many problems $\tilde{\alpha}_1$ varies only slowly with x. If it is assumed that $\tilde{\alpha}_1$ is actually independent of x, equation (92) can be simplified in the following manner:

$$L_1=\rho_\infty U_\infty \int_{-s_o}^{+s_o} \tilde{\alpha}_1 dy \int_{LE}^{TE} \frac{\Delta u_2}{\tilde{\alpha}_2} dx = \rho_\infty U_\infty \int_{-s_o}^{+s_o} \tilde{\alpha}_1 \left(\frac{\Delta\varphi_2}{\tilde{\alpha}_2}\right)_{TE} dy \tag{93}$$

Inasmuch as wing 2 in reverse flow is composed of flat-plate elements and is at zero sideslip, the circulation distribution at the trailing edge $\Delta\varphi_{TE}$ is proportional to the span loading l and equation (93) can be rewritten as

$$L_1=\int_{-s_o}^{+s_o} \tilde{\alpha}_1 \left(\frac{l_2}{\tilde{\alpha}_2}\right) dy \tag{94}$$

It is interesting to observe that this expression is identical in form with that obtained in reference 16 for planar systems of sufficiently high aspect ratio that the linear pressure-velocity relation can be used. It is important to remember, however, that the present application requires the wing in reverse flow to be at zero sideslip, whereas the analysis of reference 16 requires the wing in reverse flow to be at the same angle of sideslip as the wing in forward flow.

It is evident that equation (94) can be applied in several different ways. One can compute the total $\tilde{\alpha}_1$ induced by the vortices at the tail station, multiply by $l_2/\tilde{\alpha}_2$, and integrate by either analytical, numerical, or graphical means; or one can determine a general formula for the lift due to a single vortex and superpose the lift contributions of all the vortices. The latter method is of particular utility where the l_2 distribution is of a common form, such as elliptic. This case, which includes all low-aspect-ratio flat-plate wings having

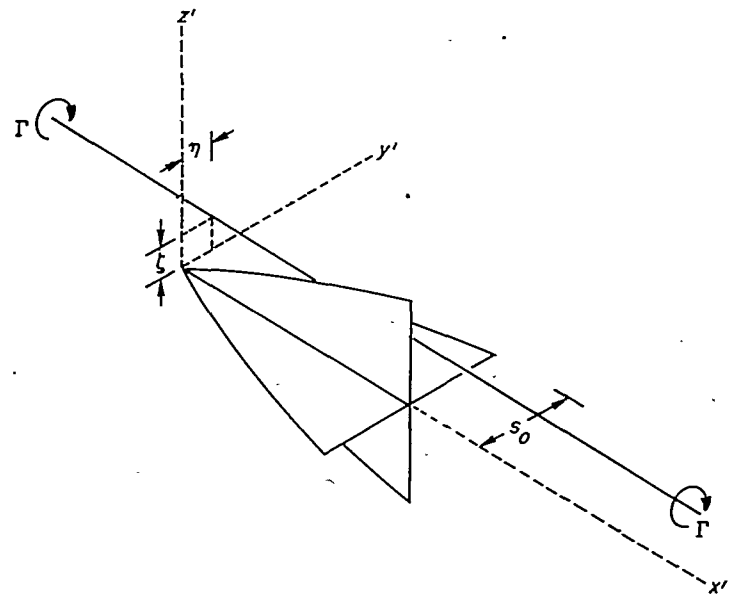

FIGURE 24.—Cruciform wing in the presence of a single vortex.

plan forms such that no part of the trailing edge lies forward of the station of maximum span, has already been treated in reference 16 but will be included here for the sake of completeness. Thus, consider the problem of determining the lift on a low-aspect-ratio cruciform wing at zero geometric angle of attack resulting from the presence of an infinite line vortex of strength Γ passing through the point $y=\eta$ and $z=\zeta$ and extending parallel to the x axis as shown in figure 24. The wing panels will be considered to have such plan forms that the span loading is elliptic when the wing is in flight in the reverse direction at zero sideslip. Thus, equation (34) yields for the wing in reverse flow

$$\frac{l_2}{\tilde{\alpha}_2}=\frac{\rho_\infty U_\infty \Delta\varphi_2}{\alpha_2}=2\rho_\infty {U_\infty}^2 \sqrt{{s_o}^2-{y_1}^2} \tag{95}$$

The effective angle of attack of the wing in forward flow is

$$\tilde{\alpha}_1=\frac{(\varphi_z)_1}{U_\infty}=-\frac{\Gamma}{2\pi U_\infty}\frac{y_1-\eta}{[y_1-\eta)^2+\zeta^2]} \tag{96}$$

Substitution of equations (95) and (96) into equation (93) or (94) yields the following formula for the lift:

$$L_1=-\Gamma\rho_\infty U_\infty s_o\left\{-\frac{\eta}{s_0}+\frac{\eta}{|\eta|}\sqrt{\frac{1}{2}\left[\sqrt{\left(1+\frac{\zeta^2}{{s_o}^2}-\frac{\eta^2}{{s_o}^2}\right)^2+\frac{4\eta^2\zeta^2}{{s_o}^4}}-\left(1+\frac{\zeta^2}{{s_o}^2}-\frac{\eta^2}{{s_o}^2}\right)\right]}\right\} \tag{97}$$

The lift on a wing in the vicinity of a number of such vortices can be found by superposition. The result so calculated applies to the wing when the geometric angle of attack α_1 is zero. If α_1 is not zero, an additional contribution must be included which is just the lift on the wing in the absence of all adjacent vortices. For the present class of plan forms, this contribution ΔL_1 can be calculated by direct application of equation (22), that is,

$$\Delta L_1=\pi\rho_\infty {U_\infty}^2 {s_o}^2 \alpha_1 \tag{98}$$

The above result may be contrasted with that of strip theory in which each section of the wing is assumed to act as though it were in two-dimensional flow at an angle of attack $\tilde{\alpha}_1$. The latter assumption results in a relation for lift of a wing in a nonuniform flow field which resembles equation (94), except that the span loading $l_2/\tilde{\alpha}_2$ is replaced with a function proportional to the local chord. Inasmuch as l_2 is not proportional, in general, to the local chord, it is evident that the use of strip theory will usually result in error.

CONCLUDING REMARKS

Several facets of the aerodynamics of slender cruciform-wing and tail interference problems have been investigated in the foregoing discussions. Formulas are given for the computation of the loading and integrated forces on cruciform wings and for the determination of the lift on a tail in an arbitrary, but known, downwash field. The principal difficulty in wing-tail interference problems resides in the determination of the flow field at the tail station and stems from the fact that the trailing vortex sheet rolls up and deforms very rapidly behind low-aspect-ratio wings. One can always compute the behavior of the vortex system within the framework of inviscid theory, but the labor is great when a sufficient number of vortices is used to give adequate representation of the actual vortex sheets. In the present study, results are given of a calculation using 40 vortices, but even this number proves insufficient to study the nature of the vortex spirals at large distances behind the wing. On the other hand, the calculations show that at sufficient distances from the wing most of the vorticity from each wing panel is concentrated within a single restricted region, and these results bear out the assumption often made that the vortex system can be represented by a much simpler model having only four vortices. If each vortex is assigned a strength equal to the total circulation around the associated wing panel, and is located, at the trailing edge, at the lateral position of the centroid of the vorticity it represents, it is shown that the lateral positions of the four vortices change with distance in such a manner that they are in close accord with the positions of the centroids of vorticity of the actual vortex system at all distances from the wing. Consequently, the lateral position of each of the four vortices is in reasonably good agreement with the lateral position of the corresponding vortex core at large distances from the wing, in spite of the fact that the 4-vortex model is clearly inadequate for representing the details of the flow at small distances from the wing.

Several aspects of the analysis of the behavior of vortex wakes remain to be investigated in future studies. In the first place, both the numerical study of the 40-vortex model and the analytical study of the 4-vortex model are confined to the case of 45° bank. Although the numerical method can be used for other bank angles and, of course, for simpler models, it does not appear possible to extend the present analytical method to other bank angles. The numerical method is slow and cumbersome, however, and there is need for other more rapid ways for calculating the form of the vortex system at the tail station. Also needed is a method for estimating the form of the vortex system in the intermediate stages of rolling up. In this range, only a part of the vorticity can logically be assumed rolled up into the vortex cores, the remainder being in the relatively undeformed sheet. A related problem exists even at great distances behind the wing where nearly all of the vorticity is concentrated in the vortex cores. Replacement of the vortex cores having finite lateral extent with line vortices of zero diameter leads to very large errors in the induced velocities at points in the immediate vicinity of the vortices. Inasmuch as the energy method used for planar wings and described in reference 1 cannot be applied directly to cases involving banked cruciform wings, there exists a need for a method for estimating the size and velocity distribution of the vortex cores so that a correction can be applied to the 4-vortex results. This need is diminished somewhat by the fact that, in many cases, the forces on the tail are not affected by the finite size of the vortex cores. This situation prevails whenever the vortex cores do not touch the tail surfaces.

AMES AERONAUTICAL LABORATORY
NATIONAL ADVISORY COMMITTEE FOR AERONAUTICS
MOFFETT FIELD, CALIF., *Oct. 25, 1955*

APPENDIX A

FORCES ON SLENDER PLANE- AND CRUCIFORM-WING AND BODY COMBINATIONS

Formulas are presented in the text of this report for the pressures and integrated forces on slender cruciform wings These results are obtained following the procedures of reference 10, but differ in that the effects of nonlinear terms in the pressure-velocity relation are now properly accounted for. Inasmuch as the inclusion of these terms also alters the pressures on cruciform-wing-body combinations, and the corrected formulas have not been given elsewhere, they will be given briefly in this appendix.

The precise problem to be discussed is that of determining the load distribution and aerodynamic properties of slender cruciform-wing and body combinations inclined at small angles of pitch, α, and yaw, β. The wing-body combination is considered to consist of a slender body of revolution and flat, pointed, low-aspect-ratio wings extending along the continuation of the horizontal and vertical meridian planes of the body as shown in figure 1. The component wings are designated wing H and wing V, as in the case of the wing alone discussed in the text. The plan form of wing H is given by $y=\pm s(x)$ and that of wing V by $z=\pm t(x)$. The radius of the body is, in general, a function of x and is designated by $r=\sqrt{y^2+z^2}=a(x)$. The analysis is confined further to wing-body combinations having wings whose edges are leading edges everywhere upstream from the base section. To extend the solutions to other configurations, further consideration must be given to the influence of the vortex wake extending downstream from the trailing edge of the wing. A brief discussion of this problem can be found in reference 17.

As described in the text, the perturbation velocity potential φ is related to the total velocity potential according to equation (1), and satisfies the Prandtl-Glauert equation given in equation (2). The general solution for slender bodies of arbitrary cross section is given in equations (3) through (6). For the present cruciform-wing and body combination, the solution must satisfy the boundary conditions given by equation (13) on the surface of the body of revolution and by equations (14) and (15) on the horizontal and vertical wings. Inasmuch as attention is confined to wings of zero thickness, the boundary conditions on the wing simplify somewhat because h is zero. Once φ is determined in this way, the pressure can be calculated directly by using the relationship given in equation (10).

Following equation (7), the solutions for φ in the vicinity of the wing-body combination can be written as

$$\varphi=\varphi_2+g(x) \tag{A1}$$

where φ_2 represents the solution of the two-dimensional Laplace equation for the specified boundary conditions and $g(x)$ is a function of x alone defined by equations (3) and (4), or explicitly by equations (8) and (9). The function φ_2 is independent of Mach number, all of the influence being confined to the function $g(x)$. As in the case of the wing alone, φ_2 can be divided into components each representing φ_2 for a simpler problem. These components are illustrated schematically in figure 25. Component φ_a represents the potential for two-dimensional incompressible flow about the wing-body cross section undergoing uniform translation in the direction of the negative z axis and is

$$\varphi_a=\pm\frac{U_\infty\alpha}{\sqrt{2}}\left\{\left[-\left(1+\frac{a^4}{r^4}\right)r^2\cos 2\theta+s^2\left(1+\frac{a^4}{s^4}\right)\right]+\left[r^4\left(1-\frac{a^4}{r^4}\right)^2+4a^4\cos^2 2\theta+s^4\left(1+\frac{a^4}{s^4}\right)^2-2s^2\left(1+\frac{a^4}{r^4}\right)\left(1+\frac{a^4}{s^4}\right)r^2\cos 2\theta\right]^{1/2}\right\}^{1/2}-U_\infty\alpha z \tag{A2}$$

where the sign is positive in the upper half-plane $0<\theta<\pi$ and negative in the lower half-plane $\pi<\theta<2\pi$. The expression for φ_b is

$$\varphi_b=\pm\frac{U_\infty\beta}{\sqrt{2}}\left\{\left[\left(1+\frac{a^4}{r^4}\right)r^2\cos 2\theta+t^2\left(1+\frac{a^4}{t^4}\right)\right]+\left[r^4\left(1-\frac{a^4}{r^4}\right)^2+4a^4\cos^2 2\theta+t^4\left(1+\frac{a^4}{t^4}\right)^2+2t^2\left(1+\frac{a^4}{t^4}\right)\left(1+\frac{a^4}{r^4}\right)r^2\cos 2\theta\right]^{1/2}\right\}^{1/2}+U_\infty\beta y \tag{A3}$$

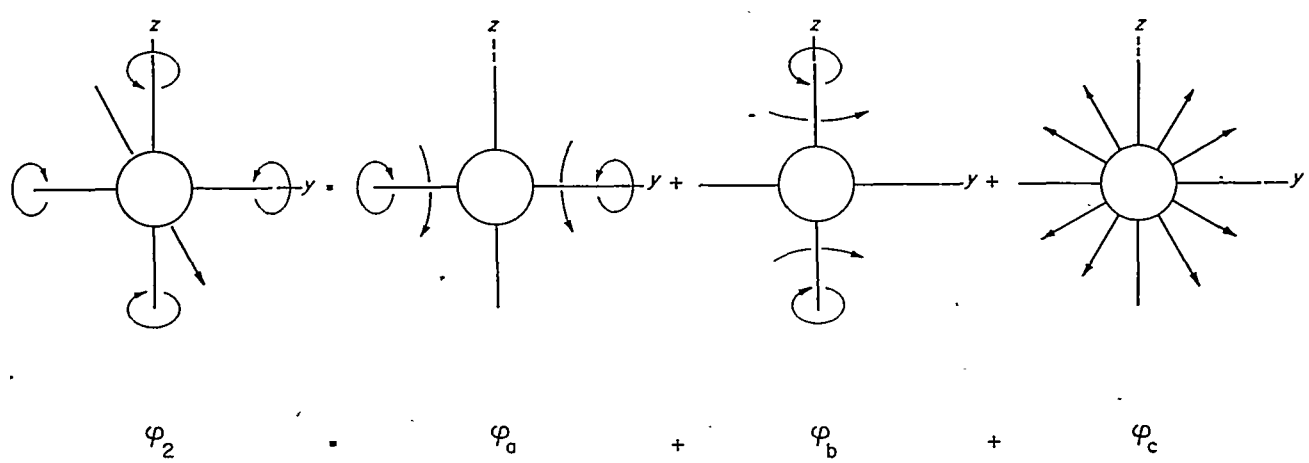

FIGURE 25.—Addition of potentials for cruciform wing-body combination

where the sign is positive in the left half-plane $\pi/2<\theta<3\pi/2$ and negative in the right half-plane $(-\pi/2<\theta<\pi/2)$. Component φ_c represents the potential for two-dimensional incompressible flow associated with a source situated at the origin and is

$$\varphi_c=\frac{U_\infty}{2\pi}\frac{dS_c}{dx}\ln r \tag{A4}$$

where $r=\sqrt{y^2+z^2}$. The perturbation velocity potential for the flow field about a cruciform-wing-body combination inclined in both pitch and yaw is

$$\varphi=\varphi_a+\varphi_b+\varphi_c+g(x) \tag{A5}$$

Through application of the above equations to the pressure-velocity relationship of equation (10), the following expressions are found for the lifting differential pressures (lower minus upper) on the horizontal wing and body

$$\left(\frac{\Delta p_L}{q}\right)_H=\frac{4\alpha\left\{\left[\frac{ds}{dx}\left(1-\frac{a^4}{s^4}\right)\right]+\frac{a}{s}\frac{da}{dx}\left[2\left(\frac{a^2}{s^2}-1\right)+\left(1-\frac{a^2}{y^2}\right)^2\right]\right\}}{\sqrt{\left(1+\frac{a^4}{s^4}\right)-\frac{y^2}{s^2}\left(1+\frac{a^4}{y^4}\right)}}+$$

$$\frac{4\alpha\beta\left(\frac{y}{s}\right)\left(1-\frac{a^4}{y^4}\right)^2}{\sqrt{\left(1+\frac{a^4}{s^4}\right)-\frac{y^2}{s^2}\left(1+\frac{a^4}{y^4}\right)}\sqrt{\frac{t^2}{y^2}\left(1+\frac{a^4}{t^4}\right)+\left(1+\frac{a^4}{y^4}\right)}} \tag{A6}$$

$$\left(\frac{\Delta p_L}{q}\right)_B=\frac{4\alpha\left[\frac{ds}{dx}\left(1-\frac{a^4}{s^4}\right)+2\frac{a}{s}\frac{da}{dx}\left(\frac{a^2}{s^2}+1-2\frac{y^2}{a^2}\right)\right]}{\sqrt{\left(1+\frac{a^2}{s^2}\right)^2-4\frac{y^2}{s^2}}}+$$

$$\frac{64\alpha\beta\left(\frac{y}{s}\right)\left(1-\frac{y^2}{a^2}\right)}{\sqrt{\left(1+\frac{a^2}{s^2}\right)^2-4\frac{y^2}{s^2}}\sqrt{\frac{t^2}{y^2}\left(1-\frac{a^2}{t^2}\right)^2+4}} \tag{A7}$$

Similarly, the lateral differential pressure (port minus starboard) on the vertical wing and body are given by

$$\left(\frac{\Delta p_Y}{q}\right)_V=-\frac{4\beta\left\{\frac{dt}{dx}\left(1-\frac{a^4}{t^4}\right)+\frac{a}{t}\frac{da}{dx}\left[2\left(\frac{a^2}{t^2}-1\right)+\left(1-\frac{a^2}{z^2}\right)^2\right]\right\}}{\sqrt{\left(1+\frac{a^4}{t^4}\right)-\frac{z^2}{t^2}\left(1+\frac{a^4}{z^4}\right)}}+$$

$$\frac{4\alpha\beta\frac{z}{t}\left(1-\frac{a^4}{z^4}\right)^2}{\sqrt{\left(1+\frac{a^4}{t^4}\right)-\frac{z^2}{t^2}\left(1+\frac{a^4}{z^4}\right)}\sqrt{\frac{s^2}{z^2}\left(1+\frac{a^4}{s^4}\right)+\left(1+\frac{a^4}{z^4}\right)}} \tag{A8}$$

$$\left(\frac{\Delta p_Y}{q}\right)_B=\frac{-4\beta\left[\frac{dt}{dx}\left(1-\frac{a^4}{t^4}\right)+2\frac{a}{t}\frac{da}{dx}\left(\frac{a^2}{t^2}+1-2\frac{z^2}{a^2}\right)\right]}{\sqrt{\left(1+\frac{a^2}{t^2}\right)^2-4\frac{z^2}{t^2}}}+$$

$$\frac{64\alpha\beta\frac{z}{t}\left(1-\frac{z^2}{a^2}\right)}{\sqrt{\left(1+\frac{a^2}{t^2}\right)^2-4\frac{z^2}{t^2}}\sqrt{\frac{s^2}{z^2}\left(1-\frac{a^2}{s^2}\right)^2+4}} \tag{A9}$$

The total lift and side force exerted on a complete cruciform-wing and body combination can be determined by integrating the loading over the entire surface area. It is often convenient to carry out the integration by first evaluating the lift and side force on one spanwise strip and then integrating these elemental forces over the length of the wing-body combination, thus

$$\frac{d}{dx}\left(\frac{L}{q}\right)=\int_{-s_o}^{+s_o}\frac{\Delta p_L}{q}dy=2\pi\alpha\frac{d}{dx}\left[s^2\left(1-\frac{a^2}{s^2}+\frac{a^4}{s^4}\right)\right] \tag{A10}$$

$$\frac{d}{dx}\left(\frac{Y}{q}\right)=\int_{-t_o}^{+t_o}\frac{\Delta p_Y}{q}dz=-2\pi\beta\frac{d}{dx}\left[t^2\left(1-\frac{a^2}{t^2}+\frac{a^4}{t^4}\right)\right] \tag{A11}$$

and

$$\frac{L}{q}=\int_0^l\frac{d}{dx}\left(\frac{L}{q}\right)dx=2\pi\alpha\left\{\left[s^2\left(1-\frac{a^2}{s^2}+\frac{a^4}{s^4}\right)\right]_l-\left[s^2\left(1-\frac{a^2}{s^2}+\frac{a^4}{s^4}\right)\right]_0\right\} \tag{A12}$$

$$\frac{Y}{q}=\int_0^l\frac{d}{dx}\left(\frac{Y}{q}\right)dx=-2\pi\beta\left\{\left[t^2\left(1-\frac{a^2}{t^2}+\frac{a^4}{t^4}\right)\right]_l-\left[t^2\left(1-\frac{a^2}{t^2}+\frac{a^4}{t^4}\right)_0\right]\right\} \tag{A13}$$

where the subscripts 0 and l in the integrated results refer to the values of the bracketed quantities at $x=0$ and $x=l$, respectively. If the wing-body combination is pointed at the nose, the bracketed quantities vanish at $x=0$, and the expressions for lift and side force reduce to

$$\frac{L}{q}=2\pi\alpha\left[s^2\left(1-\frac{a^2}{s^2}+\frac{a^4}{s^4}\right)\right]_l \tag{A14}$$

$$\frac{Y}{q}=-2\pi\beta\left[t^2\left(1-\frac{a^2}{t^2}+\frac{a^4}{t^4}\right)\right]_l \tag{A15}$$

The above expressions for the loadings and forces indicate that there is a complete correspondence of the expressions for lift and sideforce, and that the lift is independent of the angle of yaw and the side force is independent of the angle of attack. Inasmuch as the pitching and yawing moments M and N about an arbitrary moment center x_o are obtained by performing the following itegrations

$$\frac{M}{q}=-\int_0^l(x-x_o)\frac{d}{dx}\frac{L}{q}dx \tag{A16}$$

$$\frac{N}{q}=-\int_0^l(x-x_o)\frac{d}{dx}\left(\frac{Y}{q}\right)dx \tag{A17}$$

it is evident that the above statements have corresponding counterparts for these moments. Although the details of the calculation will not be given here, it can be shown further for cruciform-wing-body combinations having identical horizontal- and vertical-wing panels that the resultant lateral force $\sqrt{L^2+Y^2}$ is independent of the angle of bank, and that the total rolling moment is zero for all angles of bank.

Equations (A14) and (A15) show that the lift and side force on a slender pointed wing-body combination depend on the geometry of only the base section and not of the plan

form. This result is in conformity with the more general integral relation of equation (26) obtained using momentum methods, but not with the result obtained in reference 10 using the linear pressure-velocity relation. The latter analysis (here being superseded) indicates that equation (A14) is the proper expression for the lift of a wing-body combination consisting of a low-aspect-ratio triangular wing mounted on a slender pointed body that is cylindrical along the wing root, but not, for instance, for a conical wing-body combination. The conical configuration is of particular interest because of the existence of a supersonic conical-flow solution (ref. 18), and because it has recently been suggested (e. g., ref. 19) that that result be used to check the applicability of approximate solutions. Comparison reveals, however, that the results of reference 18 do not agree with equation (A14), but check the slender-body results of reference 10. The explanation is that the linear pressure-velocity relation is used in the supersonic conical-flow solution, and that the latter results agree with those given here if the effects of the additional terms in the pressure-velocity relation are included in the analysis.

REFERENCES

1. Spreiter, John R., and Sacks, Alvin H.: The Rolling Up of the Trailing Vortex Sheet and Its Effect on the Downwash Behind Wings. Jour. Aero. Sci., vol. 18, no. 1, Jan. 1951, pp. 21–32, 72.
2. Heaslet, Max. A., and Lomax, Harvard: Supersonic and Transonic Small Perturbation Theory. Sec. D of General Theory of High Speed Aerodynamics. Vol. VI of High Speed Aerodynamics and Jet Propulsion, W. R. Sears, series ed., Princeton Univ. Press, 1954.
3. Ward, G. N.: Linearized Theory of Steady High-Speed Flow. Cambridge Univ. Press, 1955.
4. Ward, G. N.: Supersonic Flow Past Slender Pointed Bodies. Quart. Jour. Mech. and Appl. Math., vol. II, no. 1, Mar. 1949, pp. 75–97.
5. Heaslet, Max. A., and Lomax, Harvard: The Calculation of Pressure on Slender Airplanes in Subsonic and Supersonic Flow. NACA TN 2900, 1953.
6. Keune, Friedrich: Low Aspect Ratio Wings with Small Thickness at Zero Lift in Subsonic and Supersonic Flow. Kungl. Tekniska Hogskolan, Stockholm. Institutionen för Flygteknik. Tech. Note 21, 1952.
7. Heaslet, Max. A., and Lomax, Harvard: The Calculation of Pressure on Slender Airplanes in Subsonic and Supersonic Flow. NACA Rep. 1185, 1954.
8. Oswatitsch, Klaus, and Keune, Friedrich: Ein Äquivalenzsatz für nichtangestellte Flügel kleiner Spannweite in schallnaher Strömung. Zeitschrift für Flugwissenschaften. 3 Jahr, Heft 2, Feb. 1955, S. 29–46.
9. Spreiter, John R.: Theoretical and Experimental Analysis of Transonic Flow Fields. NACA-University Conference on Aerodynamics, Construction, and Propulsion, Vol. II, Aerodynamics. A compilation of the papers presented, LFPL, Cleveland, Ohio, Oct. 20–22, 1954.
10. Spreiter, John R.: The Aerodynamic Forces on Slender Plane- and Cruciform-Wing and Body Combinations. NACA Rep. 962, 1950.
11. Durand, W. F.: Fluid Mechanics, Part I. Aerodynamic Theory, Vol. I, W. F. Durand, ed., Julius Springer (Berlin), 1935.
12. Kaden, H.: Aufwicklung einer unstabiln Unstetigkeitsflache. Ing. Archiv, II Bd., 1931, S. 140–168.
13. Westwater, F. L.: Rolling Up of the Surface of Discontinuity Behind an Aerofoil of Finite Span. R. and M. 1692, British A. R. C., Aug. 1935.
14. Rogers, Arthur W.: Application of Two-Dimensional Vortex Theory to the Prediction of Flow Fields Behind Wings of Wing-Body Combinations at Subsonic and Supersonic Speeds. NACA TN 3227, 1954.
15. Sacks, Alvin H.: Behavior of Vortex System Behind Cruciform Wings—Motions of Fully Rolled-Up Vortices. NACA TN 2605, 1952.
16. Heaslet, Max. A., and Spreiter, John R.: Reciprocity Relations in Aerodynamics. NACA Rep. 1119, 1953.
17. Adams, Mac C., and Sears, W. R.: Slender-Body Theory—Review and Extension. Jour. Aero. Sci., vol. 20, no. 2., Feb. 1953, pp. 85–98.
18. Browne, S. H., Friedman, L., and Hodes, I.: A Wing-Body Problem in a Supersonic Conical Flow. Jour. Aero. Sci., vol. 15, no. 8, Aug. 1948, pp. 443–452.
19. Lawrence, H. R., and Flax, A. H.: Wing-Body Interference at Subsonic and Supersonic Speeds—Survey and New Developments. Jour. Aero. Sci., vol. 21, no. 5, May 1954, pp. 289–324.

TABLE I.—CALCULATED LATERAL POSITIONS OF 40 VORTICES AT VARIOUS DISTANCES BEHIND A SLENDER CRUCIFORM WING AT 45° BANK

$400\sqrt{2}\frac{d}{b}\frac{C_L'}{A}$		Vortex numbers																			
		1	2	3	4	5	6	7	8	9	10	11	12	13	14	15	16	17	18	19	20
0	y'	0.2076	0.3704	0.4667	0.5367	0.5899	0.6312	0.6616	0.6828	0.7006	0.7060	0.2076	0.3704	0.4667	0.5367	0.5899	0.6312	0.6616	0.6828	0.7006	0.7060
	z'	0.2076	0.3704	0.4667	0.5367	0.5899	0.6312	0.6616	0.6828	0.7006	0.7060	−0.2076	−0.3704	−0.4667	−0.5367	−0.5899	−0.6312	−0.6616	−0.6828	−0.7006	−0.7060
1	y'	0.2078	0.3708	0.4672	0.5373	0.5905	0.6318	0.6622	0.6828	0.7021	0.6985	0.2074	0.3699	0.4661	0.5360	0.5892	0.6305	0.6609	0.6828	0.6990	0.7134
	z'	0.2080	0.3709	0.4673	0.5374	0.5907	0.6320	0.6625	0.6843	0.7006	0.7150	−0.2071	−0.3698	−0.4660	−0.5359	−0.5890	−0.6303	−0.6606	−0.6812	−0.7005	−0.6969
3	y'	0.2082	0.3718	0.4684	0.5385	0.5918	0.6333	0.6636	0.6828	0.7027	0.6857	0.2070	0.3689	0.4650	0.5348	0.5880	0.6292	0.6600	0.6833	0.7073	0.7160
	z'	0.2088	0.3721	0.4687	0.5389	0.5923	0.6337	0.6646	0.6880	0.7121	0.7207	−0.2063	−0.3686	−0.4647	−0.5345	−0.5875	−0.6288	−0.6590	−0.6781	−0.6979	−0.6909
5	y'	0.2086	0.3727	0.4695	0.5398	0.5932	0.6348	0.6654	0.6831	0.6991	0.6762	0.2065	0.3680	0.4638	0.5336	0.5868	0.6282	0.6598	0.6857	0.7173	0.7140
	z'	0.2096	0.3732	0.4700	0.5404	0.5940	0.6357	0.6675	0.6935	0.7252	0.7219	−0.2055	−0.3675	−0.4634	−0.5330	−0.5860	−0.6274	−0.6577	−0.6753	−0.6911	−0.6682
7	y'	0.2089	0.3736	0.4707	0.5411	0.5946	0.6365	0.6675	0.6837	0.6924	0.6691	0.2061	0.3671	0.4627	0.5324	0.5857	0.6274	0.6604	0.6896	0.7255	0.7110
	z'	0.2105	0.3744	0.4714	0.5420	0.5958	0.6379	0.6711	0.7004	0.7366	0 7220	−0.2047	−0.3664	−0.4621	−0.5317	−0.5845	−0.6261	−0.6568	−0.6727	−0 6812	−0.6578
11	y'	0.2097	0.3755	0.4730	0.5438	0.5975	0.6402	0.6724	0.6846	0.6759	0.6570	0.2053	0.3652	0.4605	0.5302	0.5837	0.6265	0.6632	0.7003	0.7376	0.7040
	z'	0.2122	0.3767	0.4742	0.5452	0.5996	0.6429	0.6800	0.7173	0.7549	0.7212	−0.2031	−0.3642	−0.4595	−0 5290	−0.5818	−0.6238	−0.6556	−0.6672	−0.6581	−0.6394
15	y'	0.2105	0.3774	0.4754	0.5465	0.6006	0.6441	0.6774	0.6805	0.6587	0.6500	0.2045	0.3634	0.4584	0.5281	0.5822	0.6268	0.6697	0.7143	0.7418	0.6958
	z'	0.2139	0.3792	0.4771	0.5486	0.6039	0.6492	0.6924	0.7376	0.7655	0.7192	−0.2015	−0.3621	−0.4571	−0.5263	−0.5791	−0.6218	−0.6544	−0.6560	−0.6343	−0.6260
21	y'	0.2116	0.3803	0.4790	0.5507	0.6054	0.6505	0.6836	0.6683	0.6341	0.6450	0.2032	0.3607	0.4554	0.5253	0.5807	0.6293	0.6848	0.7324	0.7400	0.6859
	z'	0.2165	0.3829	0.4817	6.5541	0.6110	0.6605	0.7164	0.7651	0.7731	0.7186	−0.1991	−0.3589	−0.4535	−0.5226	−0.5755	−0.6193	−0.6510	−0.6344	−0.5998	−0.6115
27	y'	0.2127	0.3831	0.4826	0.5551	0.6101	0.6575	0.6834	0.6515	0.6168	0.6435	0.2019	0.3580	0.4525	0.5231	0.5804	0.6350	0.7041	0.7452	0.7301	0.6801
	z'	0.2192	0.3867	0.4865	0.5601	0.6193	0.6748	0.7450	0.7875	0.7725	0.7218	−0.1968	−0.3559	−0.4500	−0.5191	−0.5721	−0.6174	−0.6409	−0.6075	−0.5718	−0.6006
33	y'	0.2138	0.3859	0.4863	0.5595	0.6156	0.6652	0.6772	0.6316	0.6044	0.6434	0.2006	0.3554	0.4499	0.5214	0.5813	0.6440	0.7225	0.7520	0.7177	0.6784
	z'	0.2220	0.3907	0.4915	0.5666	0.6257	0.6921	0.7727	0.8038	0.7693	0.7293	−0.1946	−0.3529	−0.4467	−0.5157	−0.5690	−0.6160	−0.6246	−0.5776	−0 5506	−0.5908
39	y'	0.2148	0.3888	0.4900	0.5641	0.6210	0.6728	0.6669	0.6115	0.5976	0.6426	0.1993	0.3529	0.4476	0.5203	0.5835	0.6568	0.7384	0.7525	0.7055	0.6792
	z'	0.2248	0.3948	0.4969	0.5738	0.6392	0.7129	0.7981	0.8137	0.7662	0.7397	−0.1924	−0.3501	−0.4435	−0.5125	−0 5660	−0.6139	−0.6040	−0.5475	−0.5342	−0.5805
47	y'	0.2162	0.3925	0.4950	0.5703	0.6283	0.6807	0.6492	0.5873	0.5926	0.6411	0.1975	0.3497	0.4449	0.5197	0.5881	0.6785	0.7556	0.7466	0.6905	0.6818
	z'	0.2287	0.4005	0.5043	0.5840	0.6547	0.7456	0.8282	0.8202	0.7631	0.7552	−0.1896	−0.3464	−0.4393	−0.5085	−0.5621	−0.6079	−0.5725	−0.5099	−0.5107	−0.5607
55	y'	0.2174	0.3963	0.5001	0.5766	0.6358	0.6820	0.6284	0.5681	0.5917	0.6398	0.1957	0.3467	0.4426	0.5202	0.5950	0.7034	0.7667	0.7354	0.6777	0.6800
	z'	0.2326	0.4065	0.5123	0.5952	0.6722	0.7824	0.8522	0.8212	0.7618	0.7724	−0.1868	−0.3428	−0.4354	−0.5046	−0.5582	−0.6042	−0.5379	−0.4776	−0.5032	−0.5530
63	y'	0.2187	0.4000	0.5052	0.5831	0.6435	0.6756	0.6066	0.5540	0.5944	0.6383	0.1939	0.3439	0.4410	0.5219	0.6043	0.7272	0.7718	0.7216	0.6674	0.6939
	z'	0.2367	0.4127	0.5208	0.6073	0.6918	0.8191	0.8703	0.8194	0.7631	0.7917	−0.1842	−0.3395	−0.4317	−0.5010	−0.5542	−0.5727	−0.5024	−0.4505	−0.4930	−0.5400
71	y'	0.2198	0.4037	0.5103	0.5897	0.6513	0.6633	0.5852	0.5443	0.5990	0.6356	0.1921	0.3413	0.4399	0.5247	0.6169	0.7477	0.7718	0.7069	0.6605	0.7032
	z'	0.2409	0.4191	0.5297	0.6203	0.7137	0.8531	0.8831	0.8165	0.7682	0.8124	−0.1816	−0.3362	−0.4280	−0.4974	−0.5496	−0.5454	−0.4675	−0.4281	−0.4848	−0.5250
79	y'	0.2209	0.4073	0.5154	0.5965	0.6589	0.6468	0.5653	0.5383	0.6041	0.6317	0.1904	0.3389	0.4394	0.5238	0.6300	0.7639	0.7675	0.6922	0.6567	0.7134
	z'	0.2451	0.4258	0.5391	0.6342	0.7380	0.8832	0.8913	0.8133	0.7770	0.8339	−0.1791	−0.3331	−0.4245	−0.4939	−0.5439	−0.5139	−0.4342	−0.4097	−0.4774	−0.5082
87	y'	0.2220	0.4109	0.5208	0.6033	0.6656	0.6275	0.5476	0.5357	0.6086	0.6263	0.1886	0.3368	0.4394	0.5336	0.6464	0.7766	0.7597	0.6782	0.6557	0.7240
	z'	0.2495	0.4327	0.5489	0.6489	0.7649	0.9090	0.8959	0.8107	0.7884	0.8558	−0.1767	−0.3301	−0.4211	−0.4903	−0.5364	−0.4800	−0.4032	−0.3948	−0.4699	−0.4890
95	y'	0.2229	0.4145	0.5257	0.6102	0.6706	0.6056	0.5326	0.5357	0.6125	0.6197	0.1868	0.3350	0.4401	0.5397	0.6845	0.7826	0.7493	0.6655	0.6568	0.7340
	z'	0.2539	0.4398	0.5592	0.6645	0.7943	0.9304	0.8976	0.8091	0.8016	0.8778	−0.1744	−0.3272	−0.4177	−0.4865	−0.5264	−0.4448	−0.3761	−0.3827	−0.4620	−0.4692
110	y'	0.2247	0.4211	0.5353	0.6232	0.6749	0.5661	0.5099	0.5400	0.6193	0.6047	0.1836	0.3321	0.4424	0.5532	0.7007	0.7876	0.7284	0.6447	0.6024	0.7540
	z'	0.2624	0.4537	0.5792	0.6954	0.8529	0.9624	0.8972	0.8090	0.8290	0.9187	−0.1702	−0.3220	−0.4113	−0.4790	−0.5017	−0.3783	−0.3284	−0.3644	−0.4465	−0.4284
130	y'	0.2267	0.4298	0.5482	0.6403	0.6650	0.5162	0.4932	0.5518	0.6271	0.5782	0.1795	0.3297	0.4482	0.5761	0.7469	0.7771	0.6939	0.6260	0.6778	0.7745
	z'	0.2740	0.4730	0.6078	0.7411	0.9321	0.9858	0.8940	0.8177	0.8725	0.9698	−0.1649	−0.3152	−0.4024	−0.4667	−0.4536	−0.2962	−0.2806	−0.3465	−0.4221	−0 3639
150	y'	0.2283	0.4378	0.5610	0.6563	0.6405	0.4794	0.4888	0.5657	0.6297	0.5458	0.1758	0.3291	0.4576	0.6048	0.7833	0.7534	0.6659	0.6183	0.7000	0.7844
	z'	0.2861	0.4936	0.6386	0.7929	1.0026	0.9926	0.8936	0.8380	0.9247	1.0119	−0.1600	−0.3086	−0.3929	−0.4498	−0.3919	−0.2279	−0.2474	−0.3315	−0.3895	−0.2018
170	y'	0.2296	0.4456	0.5738	0.6696	0.6081	0.4564	0.4919	0.5784	0.6284	0.5114	0.1725	0.3305	0.4701	0.6378	0.8094	0.7243	0.6440	0.6194	0.7240	0.7838
	z'	0.2984	0.5153	0.6716	0.8508	1.0630	0.9920	0.8978	0.8669	1.0816	1.0437	−0.1555	−0.3018	−0.3821	−0.4266	−0.3227	−0.1734	−0.2225	−0.3159	−0.3487	−0.2252
190	y'	0.2305	0.4530	0.5866	0.6778	0.5715	0.4446	0.4998	0.5894	0.6148	0.4788	0.1697	0.3337	0.4856	0.6733	0.8254	0.6949	0.6283	0.6275	0.7467	0.7741
	z'	0.3111	0.5379	0.7063	0.9142	1.1129	0 9903	0.9067	0.9022	1.0370	1.0653	−0.1511	−0.2946	−0.3698	−0.3959	−0.2501	−0.1309	−0.2025	−0.2981	−0.3012	−0.1580
210	y'	0.2311	0.4599	0.5993	0.6793	0.5337	0.4405	0.5115	0.5984	0.5987	0.4510	0.1676	0.3386	0.5037	0.7094	0.8323	0.6681	0.6182	0.6411	0.7662	0.7575
	z'	0.3238	0.5614	0.7440	0.9807	1.1525	0.9904	0.9205	0.9430	1.0917	1.0789	−0.1469	−0.2866	−0.3555	−0.3575	−0.1768	−0.0980	−0.1854	−0.2768	−0.2480	−0.0976
230	y'	0.2313	0.4665	0.6121	0.6735	0.4971	0.4416	0.5257	0.6045	0.5779	0.4291	0.1660	0.3453	0.5242	0.7442	0.8312	0.6453	0.6132	0.6589	0.7818	0.7361
	z'	0.3366	0.5857	0.7835	1.0478	1.1826	0.9930	0.9403	0.9881	1.1432	1.0871	−0.1426	−0.2777	−0.3390	−0.3116	−0.1049	−0.0721	−0.1699	−0.2512	−0.1923	−0.0434
250	y'	0.2313	0.4727	0.6248	0.6612	0.4638	0.4469	0.5408	0.6072	0.5536	0.4131	0.1652	0.3535	0.5468	0.7763	0.8232	0.6270	0.6130	0.6794	0.7931	0.7131
	z'	0.3495	0.6106	0.8253	1.1134	1.2043	0.9983	0.9666	1.0364	1.1906	1.0922	−0.1382	−0.2677	−0.3199	−0.2590	−0.0359	−0.0510	−0.1549	−0.2207	−0.1338	0.0032
270	y'	0.2309	0.4786	0.6374	0.6434	0.4350	0.4557	0.5548	0.6063	0.5264	0.4024	0.1650	0.3630	0.5712	0.8046	0.8097	0.6130	0.6177	0.7012	0.8000	0.6897
	z'	0.3623	0.6362	0.8695	1.1760	1.2193	1.0068	0.9996	1.0363	1.2332	1.0957	−0.1334	−0.2564	−0.2980	−0.2007	0.0289	−0.0331	−0.1395	−0.1852	−0.0742	0.0428
290	y'	0.2303	0.4840	0.6497	0.6214	0.4116	0.4674	0.5660	0.6020	0.4975	0.3964	0.1655	0.3738	0.5971	0.8233	0.7919	0.6030	0.6270	0.7230	0.8028	0.6675
	z'	0.3749	0.6623	0.9162	1.2349	1.2295	1.0189	1.0382	1.1369	1.2703	1.0986	−0.1281	−0.2438	−0.2732	−0.1380	0.0889	−0.0176	−0.1224	−0.1450	−0.0140	0.0701
310	y'	0.2294	0.4891	0.6612	0.5960	0.3935	0.4813	0.5735	0.5946	0.4680	0.3948	0.1667	0.3856	0.6244	0.8470	0.7710	0.5963	0.6404	0.7436	0.8018	0.6476
	z'	0.3874	0.6889	0.9654	1.2895	1.2366	1.0352	1.0809	1.1875	1.3015	1.1016	−0.1223	−0.2297	−0.2453	−0.0722	0.1435	−0.0035	−0.1024	−0.1007	0.0441	0.1041
330	y'	0.2282	0.4938	0.6716	0.5679	0.3804	0.4965	0.5769	0.5846	0.4392	0.3970	0.1684	0.3984	0.6529	0.8606	0.7482	0.5944	0.6567	0.7625	0.7975	0.6305
	z'	0.3997	0.7159	1.0171	1.3397	1.2420	1.0562	1.1261	1.2375	1.3268	1.1055	−0.1167	−0.2142	−0.2142	−0.0044	0.1923	0.0097	−0.0785	−0.0532	0.1014	0.1279
350	y'	0.2269	0.4982	0.6802	0.5378	0.3715	0.5121	0.5763	0.5720	0.4124	0.4027	0.1708	0.4120	0.6822	0.8693	0.7246	0.5957	0.6748	0.7794	0.7903	0.6164
	z'	0.4117	0.7434	1.0713	1.3848	1.2469	1.0820	1.1722	1.2867	1.3465	1.1108	−0.1083	−0.1973	−0.1798	0.0643	0.2361	0.0226	−0.0502	−0.0030	0.1563	0.1484
370	y'	0.2255	0.5024	0.6866	0.5065	0.3862	0.5271	0.5736	0.5572	0.3884	0.4115	0.1738	0.4264	0.7119	0.8733	0.7012	0.6006	0.6935	0.7942	0.7807	0.6055
	z'	0.4235	0.7712	1.1277	1.4248	1.2518	1.1124	1.2184	1.3347	1.3615	1.1183	−0.1001	−0.1790	−0.1420	0.1331	0.2723	0.0359	−0.0174	0.0491	0.2100	0.1664
390	y'	0.2240	0.5063	0.6902	0.4748	0.3641	0.5409	0.5679	0.5403	0.3677	0.4229	0.1772	0.4413	0.7418	0.8729	0.6790	0.6090	0.7118	0.8070	1.7691	0.5978
	z'	0.4348	0.7993	1.1860	1.4593	1.2572	1.1469	1.2638	1.3814	1.3726	1.1286	−0.0909	−0.1593	−0.1007	0.2014	0.3038	0.0501	0.0194	0.1031	0.2606	0.1828
410	y'	0.2224	0.5099	0.6909	0.4435	0.3646	0.5532	0.5602	0.5216	0.3506	0.4364	0.1811	0.4569	0.7712	0.8685	0.6588	0.6209	0.7288	0.8178	0.7560	0.5930
	z'	0.4459	0.8277	1.2456	1.4881	1.2635	1.1848	1.3081	1.4265	1.3808	1.1423	−0.0807	−0.1383	−0.0557	0.2684	0.3304	0.0658	0.0588	0.1584	0.3080	0.1980
430	y'	0.2208	0.5134	0.6883	0.4135	0.3674	0.5638	0.5508	0.5011	0.3369	0.4512	0.1855	0.4730	0.7996	0.8603	0.6415	0.6362	0.7440	0.8260	0.7416	0.5912
	z'	0.4566	0.8564	1.3061	1.5113	1.2708	1.2256	1.3512	1.4698	1.3869	1.1599	−0.0696	−0.1161	−0.0072	0.3337	0.3528	0.0837	0.1030	0.2148	0.3536	0.2127

TABLE I.—CALCULATED LATERAL POSITIONS OF 40 VORTICES AT VARIOUS DISTANCES BEHIND A SLENDER CRUCIFORM WING AT 45° BANK—Continued

$400\sqrt{2}\frac{d}{b}\frac{C_L'}{A}$		Vortex numbers																			
		1	2	3	4	5	6	7	8	9	10	11	12	13	14	15	16	17	18	19	20
450	y'	0.2193	0.5166	0.6823	0.3859	0.3723	0.5726	0.5401	0.4789	0.3266	0.4666	0.1902	0.4896	0.8265	0.8487	0.6274	0.6545	0.7571	0.8323	0.7263	0.5921
	z'	0.4669	0.8854	1.3667	1.5292	1.2796	1.2689	1.3926	1.5112	1.3915	1.1816	−0.0574	−0.0927	0.0446	0.3966	0.3718	0.1044	0.1480	0.2721	0.3955	0.2271
470	y'	0.2179	0.5197	0.6730	0.3615	0.3788	0.5797	0.5282	0.4551	0.3191	0.4821	0.1953	0.5066	0.8515	0.8342	0.6168	0.6755	0.7682	0.8364	0.7106	0.5957
	z'	0.4770	0.9145	1.4269	1.5423	1.2900	1.3143	1.4323	1.5502	1.3952	1.2076	−0.0443	−0.0681	0.0999	0.4565	0.3886	0.1285	0.1942	0.3299	0.4340	0.2416
490	y'	0.2167	0.5227	0.6605	0.3412	0.3868	0.5849	0.5156	0.4295	0.3144	0.4970	0.2007	0.5239	0.8740	0.8173	0.6096	0.6987	0.7774	0.8383	0.6950	0.6021
	z'	0.4868	0.9437	1.4861	1.5515	1.3023	1.3615	1.4702	1.5863	1.3984	1.2377	−0.0303	−0.0425	0.1580	0.5131	0.4042	0.1563	0.2410	0.3881	0.4692	0.2566
510	y'	0.2156	0.5254	0.6449	0.3252	0.3958	0.5882	0.5025	0.4025	0.3121	0.5108	0.2064	0.5416	0.8938	0.7986	0.6053	0.7234	0.7848	0.8380	0.6801	0.6110
	z'	0.4964	0.9730	1.5437	1.5583	1.3166	1.4104	1.5062	1.6185	1.4013	1.2718	−0.0152	−0.0157	0.2187	0.5659	0.4192	0.1882	0.2881	0.4462	0.5011	0.2724
530	y'	0.2149	0.5278	0.6266	0.3130	0.4058	0.5894	0.4891	0.3750	0.3121	0.5233	0.2123	0.5595	0.9106	0.7789	0.6036	0.7490	0.7906	0.8356	0.6663	0.6226
	z'	0.5053	1.0024	1.5993	1.5638	1.3332	1.4607	1.5403	1.6462	1.4043	1.3097	0.0006	0.0120	0.2814	0.6147	0.4340	0.2241	0.3352	0.5040	0.5301	0.2894
550	y'	0.2144	0.5300	0.6058	0.3041	0.4164	0.5885	0.4757	0.3481	0.3142	0.5339	0.2184	0.5778	0.9241	0.7586	0.6041	0.7750	0.7951	0.8312	0.6539	0.6368
	z'	0.5151	1.0320	1.6524	1.5689	1.3522	1.5120	1.5728	1.6691	1.4074	1.3511	0.0174	0.0409	0.3457	0.6594	0.4491	0.2641	0.3819	0.5612	0.5565	0.3082
570	y'	0.2143	0.5320	0.5829	0.2978	0.4274	0.5852	0.4625	0.3227	0.3183	0.5421	0.2248	0.5963	0.9342	0.7385	0.6068	0.8007	0.7984	0.8249	0.6430	0.6533
	z'	0.5244	1.0616	1.7026	1.5740	1.3738	1.5640	1.6036	1.6875	1.4110	1.3954	0.0350	0.0708	0.4110	0.7002	0.4644	0.3081	0.4281	0.6175	0.5807	0.3292

TABLE II.—CALCULATED LATERAL POSITIONS OF CENTROIDS OF VORTICITY OF 40 VORTICES BEHIND A SLENDER CRUCIFORM WING AT 45° BANK

$400\sqrt{2}\frac{d}{b}\frac{C_L'}{A}$		Vortex numbers		$400\sqrt{2}\frac{d}{b}\frac{C_L'}{A}$		Vortex numbers		$400\sqrt{2}\frac{d}{b}\frac{C_L'}{A}$		Vortex numbers		$400\sqrt{2}\frac{d}{b}\frac{C_L'}{A}$		Vortex numbers	
		1 to 10	11 to 20			1 to 10	11 to 20			1 to 10	11 to 20			1 to 10	11 to 20
0	y_c'	0.5551	0.5554	47	y_c'	0.5454	0.5653	190	y_c'	0.5147	0.5960	410	y_c'	0.4654	0.6453
	z_c'	0.5564	−0.5554		z_c'	0.6284	−0.4820		z_c'	0.8484	−0.2553		z_c'	1.1714	0.1115
1	y_c'	0.5551	0.5556	55	y_c'	0.5437	0.5670	210	y_c'	0.5104	0.6003	430	y_c'	0.4608	0.6499
	z_c'	0.5569	−0.5537		z_c'	0.6408	−0.4695		z_c'	0.8787	−0.2230		z_c'	1.1995	0.1461
3	y_c'	0.5547	0.5560	63	y_c'	0.5420	0.5687	230	y_c'	0.5060	0.6047	450	y_c'	0.4562	0.6545
	z_c'	0.5600	−0.5506		z_c'	0.6532	−0.4570		z_c'	0.9088	−0.1905		z_c'	1.2274	0.1810
5	y_c'	0.5543	0.5564	71	y_c'	0.5403	0.5704	250	y_c'	0.5016	0.6091	470	y_c'	0.4516	0.6591
	z_c'	0.5631	−0.5475		z_c'	0.6657	−0.4443		z_c'	0.9387	−0.1578		z_c'	1.2550	0.2160
7	y_c'	0.5539	0.5568	79	y_c'	0.5386	0.5721	270	y_c'	0.4971	0.6136	490	y_c'	0.4470	0.6637
	z_c'	0.5662	−0.5444		z_c'	0.6781	−0.4217		z_c'	0.9685	−0.1248		z_c'	1.2824	0.2513
11	y_c'	0.5530	0.5577	87	y_c'	0.5369	0.5738	290	y_c'	0.4927	0.6180	510	y_c'	0.4424	0.6683
	z_c'	0.5724	−0.5382		z_c'	0.6905	−0.4192		z_c'	0.9981	−0.0917		z_c'	1.3097	0.2869
15	y_c'	0.5522	0.5585	95	y_c'	0.5352	0.5756	310	y_c'	0.4882	0.6225	530	y_c'	0.4378	0.6729
	z_c'	0.5787	−0.5319		z_c'	0.7029	−0.4066		z_c'	1.0275	−0.0584		z_c'	1.3366	0.3226
21	y_c'	0.5509	0.5598	110	y_c'	0.5320	0.5788	330	y_c'	0.4836	0.6270	550	y_c'	0.4332	0.6775
	z_c'	0.5880	−0.5226		z_c'	0.7260	−0.3830		z_c'	1.0566	−0.0249		z_c'	1.3633	0.3585
27	y_c'	0.5496	0.5611	130	y_c'	0.5277	0.5830	350	y_c'	0.4791	0.6316	570	y_c'	0.4286	0.6821
	z_c'	0.5973	−0.5132		z_c'	0.7568	−0.3512		z_c'	1.0856	0.0088		z_c'	1.3898	0.3945
33	y_c'	0.5493	0.5624	150	y_c'	0.5234	0.5873	370	y_c'	0.4745	0.6362				
	z_c'	0.6057	−0.5039		z_c'	0.7875	−0.3194		z_c'	1.1144	0.0428				
39	y_c'	0.5471	0.5636	170	y_c'	0.5191	0.5916	390	y_c'	0.4700	0.6407				
	z_c'	0.6160	−0.4945		z_c'	0.8180	−0.2874		z_c'	1.1430	0.0771				